Systems/Circuits

mGluR5 in Astrocytes in the Ventromedial Hypothalamus Regulates Pituitary Adenylate Cyclase-Activating Polypeptide Neurons and Glucose Homeostasis

Alice Meng,[1] Dominique Ameroso,[2] and Maribel Rios[1,2,3]

[1]Graduate Program in Cell, Molecular and Developmental Biology, Graduate School of Biomedical Sciences, Tufts University School of Medicine, Boston, Massachusetts 02111, [2]Graduate Program in Neuroscience, Graduate School of Biomedical Sciences, Tufts University School of Medicine, Boston, Massachusetts 02111, United States, and [3]Department of Neuroscience, Tufts University School of Medicine, Boston, Massachusetts 02111

The ventromedial hypothalamus (VMH) is a functionally heterogeneous nucleus critical for systemic energy, glucose, and lipid balance. We showed previously that the metabotropic glutamate receptor 5 (mGluR5) plays essential roles regulating excitatory and inhibitory transmission in SF1$^+$ neurons of the VMH and facilitating glucose and lipid homeostasis in female mice. Although mGluR5 is also highly expressed in VMH astrocytes in the mature brain, its role there influencing central metabolic circuits is unknown. In contrast to the glucose intolerance observed only in female mice lacking mGluR5 in VMH SF1 neurons, selective depletion of mGluR5 in VMH astrocytes enhanced glucose tolerance without affecting food intake or body weight in both adult female and male mice. The improved glucose tolerance was associated with elevated glucose-stimulated insulin release. Astrocytic mGluR5 male and female mutants also exhibited reduced adipocyte size and increased sympathetic tone in gonadal white adipose tissue. Diminished excitatory drive and synaptic inputs onto VMH Pituitary adenylate cyclase-activating polypeptide (PACAP$^+$) neurons and reduced activity of these cells during acute hyperglycemia underlie the observed changes in glycemic control. These studies reveal an essential role of astrocytic mGluR5 in the VMH regulating the excitatory drive onto PACAP$^+$ neurons and activity of these cells facilitating glucose homeostasis in male and female mice.

Key words: **astrocytes; glucose; glutamate; hypothalamus; mGluR5**

Significance Statement

Neuronal circuits within the VMH play chief roles in the regulation of whole-body metabolic homeostasis. It remains unclear how astrocytes influence neurotransmission in this region to facilitate energy and glucose balance control. Here, we explored the role of the metabotropic glutamate receptor, mGluR5, using a mouse model with selective depletion of mGluR5 from VMH astrocytes. We show that astrocytic mGluR5 critically regulates the excitatory drive and activity of PACAP-expressing neurons in the VMH to control glucose homeostasis in both female and male mice. Furthermore, mGluR5 in VMH astrocytes influences adipocyte size and sympathetic tone in white adipose tissue. These studies provide novel insight toward the importance of hypothalamic astrocytes participating in central circuits regulating peripheral metabolism.

Introduction

Global prevalence of obesity and associated metabolic disorders, such as diabetes, continues to rise, presenting a substantial clinical burden. Alterations in complex neuronal circuits within the hypothalamus are thought to contribute as they play key roles in the maintenance of whole-body metabolic homeostasis. Accordingly, they orchestrate physiological and behavioral responses that accommodate the energy and glycemic requirements of the animal, including changes in food intake, energy expenditure, and glucose production and utilization. The ventromedial hypothalamus (VMH) is a primarily glutamatergic nucleus that participates prominently in these metabolic processes. It contains subpopulations of neurons that are functionally diverse and mediate glucose homeostasis via opposing mechanisms (King, 2006; Shimazu and Minokoshi, 2017; Tu et al., 2022). Although previous investigations have focused on those cells, far less is known about the roles played by VMH astrocytes influencing energy and glucose balance.

Received Feb. 1, 2023; revised May 9, 2023; accepted July 16, 2023.

Author contributions: A.M. and M.R. designed research; A.M. and D.A. performed research; A.M., D.A., and M.R. analyzed data; and A.M. and M.R. wrote the paper.

This work was supported by National Institutes of Health (NIH)–National Institute of Diabetes and Digestive and Kidney Diseases Grants R01DK117935 and R01DK113445 (to M.R.), 1T32DK124170-01 (to A.M.), and 1F31DK118789-01A1 (to D.A.). We thank the Vanderbilt Hormone Assay and Analytical Services Core, supported by NIH Grant DK020593 (to Vanderbilt Diabetes Research and Training Center), for assistance with tissue norepinephrine and triglyceride analysis.

The authors declare no competing financial interests.

Correspondence should be addressed to Maribel Rios at maribel.rios@tufts.edu.

https://doi.org/10.1523/JNEUROSCI.0193-23.2023

We reported previously a female-specific role for the metabotropic glutamate receptor 5 (mGluR5) in $SF1^+$ neurons in the VMH of mice, mediating glucose and lipid homeostasis in a manner independent of energy balance control. mGluR5 is a group I metabotropic glutamate receptor that regulates synaptic plasticity and excitatory neurotransmission across the brain. In the VMH it augments and reduces the excitatory and inhibitory drive, respectively, onto $SF1^+$ neurons to facilitate glucose and lipid balance in female mice (Fagan et al., 2020). Ultrastructural studies in rat VMH indicate that mGluR5 is also expressed in astrocytic processes that are in close apposition with excitatory synapses in this region (Van Den Pol et al., 1995). In other brain areas, it serves as an extracellular glutamate-sensing receptor in astrocytes where it increases intracellular Ca^{2+} to facilitate astrocytic regulation of synaptic transmission (Panatier et al., 2011; Sun et al., 2014). Indeed, astrocytic mGluR5 has been linked to gliotransmitter release, synaptic glutamate clearance, and remodeling of perisynaptic astrocytic processes (Vermeiren et al., 2005; D'Ascenzo et al., 2007; Lavialle et al., 2011; Panatier et al., 2011; Devaraju et al., 2013; Bernardinelli et al., 2014). The prevailing opinion, stemming largely from cortical and hippocampal studies, is that astrocytic mGluR5 expression is confined to development and the early postnatal period (Cai et al., 2000; Sun et al., 2013; Morel et al., 2014). The significance of the persistent mGluR5 expression in astrocytes in the adult VMH and its potential role regulating neuronal activity and metabolic homeostasis has not been explored.

Astrocytic processes contact thousands of synapses and can rapidly remodel to engage or disengage them, influencing their stability and neuronal activity (Oliet et al., 2001; Bushong et al., 2002; Halassa et al., 2007; Bernardinelli et al., 2014). The role of astrocytes regulating central metabolic circuits remains vastly understudied. In the arcuate nucleus of the hypothalamus, they express receptors for metabolic hormones such as leptin and insulin, and loss of these astrocytic receptors disrupts feeding and homeostatic responses to altered peripheral glucose availability, respectively (Kim et al., 2014; García-Cáceres et al., 2016). We recently reported an essential role for BDNF/TrkB.T1 signaling in VMH astrocytes mediating the effects of energy status on astrocytic function, excitatory transmission, and energy and glucose homeostasis (Ameroso et al., 2022).

Here, we investigated the role of astrocytic mGluR5 in the regulation of excitatory neurotransmission in the VMH and systemic metabolic homeostasis. We show that in contrast to its actions in $SF1^+$ neurons, selective depletion of mGluR5 from VMH astrocytes improves glucose tolerance in both male and female mice. These metabolic changes are associated with diminished excitatory drive and activity of VMH pituitary adenylate cyclase activating polypeptide ($PACAP^+$) neurons, which normally inhibit insulin secretion. Collectively, our findings reveal a novel and essential role for mGluR5 within VMH astrocytes driving PACAP neuronal activity to facilitate glucose homeostasis.

Materials and Methods

Animals

All procedures were approved by the institutional Animal Care and Use Committee at Tufts University and conducted in accordance with the National Institutes of Health *Guide for Care and Use of Laboratory Animals*. Mice were housed in a 14/10 h dark/light cycle with an ambient temperature of 20–23°C and 30–70% humidity with water and chow *ad libitum* (18.6% protein, 6.2% fat and a caloric content of 3.1 kcal/g; catalog #2918, Envigo) unless otherwise indicated. For experiments involving fasting, mice were food restricted for 16 h with water *ad libitum*. Mice with VMH astrocyte-specific mGluR5 depletion were generated using floxed mGluR5 mice in a C57BL6 background as described below. For electrophysiology experiments, mice containing floxed mGluR5 alleles were crossed to mice with Cre-dependent expression of tdTomato (strain #007914) obtained from The Jackson Laboratory. All experiments were performed in both male and female mice, using littermates and age-matched animals to reduce variability.

Stereotaxic surgeries

Stereotaxic surgeries were performed in male and female floxed mGluR5 mice (strain #028626, The Jackson Laboratory) or floxed mGluR5 mice crossed to tdTomato mice at 8–12 weeks of age. For electrophysiological experiments, surgeries were performed at 7–8 weeks of age. Animals were anesthetized by isoflurane inhalation using the Kent Scientific SomnoSuite Low-Flow Isoflurane Anesthesia system. The VMH was bilaterally targeted using stereotaxic coordinates AP, −1.20; ML, ±0.50; DV −5.75 from bregma. Viruses were obtained from the University of North Carolina Viral Vector Core. Adeno-associated virus (AAV)5-GFAP-eGFP (100 nl, $3 \times 10^{a}8$ viral particles per side) and AAV5-GFAP-eGFP-Cre (125 nl, $3 \times 10^{a}8$ viral particles per side) were delivered to generate control and mutant mice with VMH astrocyte-specific mGluR5 depletion, respectively. *Post hoc* analysis was performed in every animal to confirm targeting of the VMH using immunofluorescent labeling of GFP expression and/or tdTomato expression in the VMH, and mistargeted animals were excluded from the analyses.

Immunofluorescence

Mice were anesthetized with isoflurane and perfused with 4% paraformaldehyde in 1× PBS. Brains were extracted and postfixed in 4% paraformaldehyde for 18–24 h at 4°C followed by cryoprotection in 30% sucrose solution and optimal cutting temperature compound embedding. Free-floating coronal sections (30 μm thick) were collected using a Leica CM1900 cryostat. For confirmation of astrocytic mGluR5 expression and viral transduction specificity, sections were blocked in 5% NGS and 0.3% Triton X-100 in 1× PBS 1 h at room temperature followed by incubation with primary antibodies in blocking buffer overnight at 4°C. The following primary antibodies were used: rabbit anti-mGluR5 (1:3000; catalog #AB5675, Millipore) chicken anti-GFP (1:800; catalog #ab13970, Abcam), mouse anti-NeuN (1:250; catalog #MAB377, Millipore), and rabbit anti-Sox9 (1:1000; catalog #AB5535, Millipore). Sections were incubated in secondary antibodies in blocking buffer (goat anti-chicken Alexa Fluor 488, goat anti-rabbit Cy3, goat anti-mouse Alexa Fluor 647; 1:500; Jackson ImmunoResearch) for 1 h at room temperature, followed by mounting with DAPI-Fluoromount G (Southern Biotech) and coverslipping. A Nikon A1R confocal microscope was used to capture *Z*-stack images. Colocalization of GFP expression with mGluR5, NeuN, or Sox9 was determined using ImageJ software.

RNAscope

Brains were extracted and processed as described for the immunofluorescence studies. Cryosections (12 μm thick) were obtained, dry mounted onto charged slides, and stored at −80°C until processing. The RNAscope Fluorescent Multiplex Reagent Kit (ACD Bio) was used per instructions from the manufacturer using mGluR5 (Mm-GRM5-C2) and Sox9 (Mm-Sox9-C3) probes. VMH images were acquired on a Nikon A1R microscope at 40× magnification.

Western blots

Mice were killed at 5–6 weeks post-surgery and their brains removed for isolation of VMH tissue. Eight-hundred-micrometer coronal slices spanning the rostrocaudal extent of the VMH were obtained using a Leica VT1000 S Vibratome, and the VMH was microdissected using a dissecting scope and flash frozen. VMH tissue was lysed in T-PER Tissue Protein Extraction Reagent (catalog #78510, Thermo Fisher Scientific) containing Halt Protease/Phosphatase Inhibitor Cocktail (catalog #78440, Thermo Fisher Scientific). Lysates were sonicated and centrifuged at 14 000 × *g* for 8 min, and the supernatant was collected. Protein

concentration was quantified using the Pierce BCA Protein Assay Kit (catalog #23225, Thermo Fisher Scientific). Samples were reduced in a 5× β-mercaptoethanol-based loading buffer (1 ml glycerol, 1 g SDS, 3.1 ml 1 M Tris, pH 6.8, 100 μl 5% bromophenol blue, 2.5 ml β-mercaptoethanol, and dH20) for 30 min at room temperature or 5 min at 95°C. Protein samples (10 μg) were run on 4–12% Tris-glycine gels (catalog #XP04122BOX, Thermo Fisher Scientific) and transferred to PVDF membranes. Membranes were blocked in 5% milk in 1× TBST for 1 h at room temperature. Primary antibodies were incubated in blocking buffer overnight at 4°C, and secondary antibodies were incubated in blocking buffer for 1 h at room temperature. Blots were developed using ECL Prime (catalog #RPN2232, Cytiva) onto HyBlot ES autoradiography film (catalog #1156P37, Thomas Scientific). Densitometry was performed using ImageJ software.

The following primary antibodies were used: rabbit anti-mGluR5 (1:1000; catalog #55920, Cell Signaling Technology), rabbit anti-β-tubulin (1:20,000; catalog #ab6046, Abcam), mouse anti-TSP-1 (1:250; catalog #sc59887, Santa Cruz Biotechnology), rabbit anti-TSP-2 (1:1000; catalog #ab84469, Abcam), goat anti-hevin (1:4000; catalog #AF2836-SP, R&D Systems), rabbit anti-glypican-4 (1:250; catalog #13048-1-AP, Proteintech), mouse anti-β-actin (1:50,000; catalog #A1978, Sigma-Aldrich), mouse anti-ezrin (1:250; catalog #sc58758, Santa Cruz Biotechnology), and mouse anti-GLT-1 (1:3000; catalog #MAB2262, EMD Millipore). The following secondary antibodies were used: anti-rabbit IgG HRP (catalog #7074, Cell Signaling Technology), anti-mouse IgG HRP (catalog #7076, Cell Signaling Technology), and anti-goat IgG HRP (catalog #HAF109, R&D Systems).

Food intake and body weight measurements

Following stereotaxic surgeries, mice were individually housed with water and chow *ad libitum*. Body weights were measured weekly after surgery at the same time of day. Weekly food intake was measured during weeks 3–6 after surgery by providing a premeasured amount of food and weighing the food remaining at the end of the week. For body weight measurements during dietary challenge, animals were administered a high-fat diet (45% kcal fat, 20% kcal protein, 35% kcal carbohydrate, and a caloric content of 4.7 kcal/g; catalog #D12451, Research Diets) beginning at 14 weeks post-surgery, and body weights were measured weekly for a total of 16 weeks.

Glucose and insulin tolerance tests

Glucose tolerance tests (GTTs) and insulin tolerance tests (ITTs) were performed at 9–11 weeks post-surgery. Mice were fasted for 16 h or 6 h for glucose and insulin tolerance tests, respectively. Blood glucose levels (mg/dl) were measured using the Freestyle Blood Glucose Monitoring System (Abbott Diabetes Care) from blood droplets obtained from a lateral nick in the tail. Following a baseline measurement at time zero, 1.5 g/kg of D-glucose (for GTTs) or 0.85 U/kg insulin (for ITTs; Humulin R U-100) was administered intraperitoneally. For GTTs, blood glucose was measured at 15, 30, 60, and 120 min after injection; for ITTs, blood glucose was measured at 15, 30, 60, 90, and 120 min after injection.

Serum insulin and glucagon measurements

To measure serum insulin levels, blood was collected from the trunk or submandibular vein of mice fasted for 16 h, and serum was isolated using BD Microtainer tubes (catalog #365967, Thermo Fisher Scientific). For experiments measuring glucose-stimulated insulin secretion, mice were intraperitoneally injected with 1.5 g/kg body weight D-glucose following fasting and killed 8 min later. Serum insulin content was quantified using the Rat/Mouse Insulin ELISA kit (catalog #EZRMI-13K MilliporeSigma). Baseline fasted and glucose-stimulated measurements were performed at 16–18 weeks and 11 weeks post-surgery, respectively.

Glucagon levels in serum were measured in mice that were fasted for 6 h and intraperitoneally injected with 0.85 U/kg insulin at 11 weeks post-surgery. Mice were killed 75 min after insulin injection, and trunk blood was collected into BD Microtainer tubes for isolation of serum. Serum glucagon content was quantified by the Mercodia Glucagon ELISA kit (catalog #10-1281-01).

Norepinephrine measurements

Serum, liver, perigonadal, and inguinal white adipose tissue (iWAT); interscapular brown adipose tissue; and skeletal muscle were collected from animals at 20 weeks after surgery. Serum was treated with EGTA-glutathione at the time of collection and stored at −80°C. Tissues were flash frozen in liquid nitrogen and homogenized with 5 mM glutathione/0.4 N perchloric acid solution (1 ml/100 mg tissue). Norepinephrine content was measured by the Vanderbilt Hormone Assay and Analytical Services Core using HPLC.

Adipocyte size measurements

Gonadal white adipose tissue was harvested from mice at 30 weeks post-surgery and fixed in 10% neutral buffered formalin. Paraffin embedding and hematoxylin and eosin staining was performed by the Tufts Animal Histology Core. Brightfield images were acquired on a Nikon E800 microscope at 10× magnification. Adipocyte cell size was measured using the ImageJ plug-in Adiposoft from three images per animal.

Lipid measurements

Serum was collected from fed and fasted animals at 18–20 weeks post-surgery, and circulating levels of glycerol and free fatty acids (FFAs) were measured using colorimetric assays (catalog #MAK117 and #MAK044, MilliporeSigma). Triglyceride concentration was measured in perigonadal white adipose tissue by the Vanderbilt Hormone Assay and Analytical Services Core using gas chromatography.

Analysis of c-fos expression after glucose administration

Mice were fasted for 16 h and injected intraperitoneally with 1.5 g/kg body weight D-glucose. At 60 min following glucose injection, animals were perfused with 4% paraformaldehyde and processed for immunofluorescence staining as previously described. Then 30 μm free-floating coronal sections were blocked in 1% BSA, 5% NDS, 0.4% Triton X-100 in 1× PBS for 1 h at room temperature and incubated overnight at 4°C in with chicken anti-GFP, goat anti-c-fos (1:200; catalog #SC-52-G, Santa Cruz Biotechnology) and rabbit anti-PACAP (1:500; catalog #bs0190-R, Bioss), followed by secondary antibodies donkey anti-chicken Alexa Fluor 488, donkey anti-goat Cy3, donkey anti-rabbit Alexa Fluor 647 (1:500; Jackson ImmunoResearch). *Z*-stacks of the VMH were captured using a Nikon A1R confocal microscope at 20×. The number of c-fos$^+$ cells and colocalization with PACAP expression were analyzed in two sections per animal using ImageJ software.

Quantification of synapse density

Brains were processed for immunofluorescence staining as previously described. For excitatory synapse density, sections were postfixed for 10 min in 4% PFA at room temperature and blocked for 30 min in 10% NGS, 1% milk, and 0.5% Triton X-100 in 1× PBS. Sections were then incubated with guinea pig anti-VGLUT2 (1:1000; catalog #AB2251; Millipore) and rabbit anti-PSD95 (1:500; catalog #51-6900. Invitrogen) overnight at 4°C followed by incubation with secondary antibodies (goat anti-rabbit Cy3 and goat anti-guinea pig Alexa Fluor 647; 1:500; Jackson ImmunoResearch) for 2 h at room temperature. Images of the VMH (three per side corresponding to the dorsomedial, central, and ventrolateral subregions) were acquired with a Nikon A1R confocal at 64× magnification. Colocalization of vGlut2 and PSD95 was quantified using the Synapse Counter plug-in in ImageJ.

To quantify excitatory inputs onto PACAP$^+$ cells, sections were blocked with 1% BSA, 5% NGS, 0.4% Triton X-100 in 1× PBS and coimmunolabeled overnight at 4°C with anti-vGlut2, anti-PACAP and anti-NeuN (1:1000; catalog #ab104224, Abcam) followed by incubation with secondary antibodies for 1 h at room temperature. *Z*-stack images were acquired on a Nikon A1R confocal at 64×, and three-dimensional reconstructions of PACAP$^+$ cell soma were generated with the Surfaces tool in Imaris Image Analysis Software using the NeuN stain to fill the cell body. vGlut2 puncta within the volume of the PACAP$^+$ cell soma were counted using the Spots function in Imaris.

The following primary antibodies were used: guinea pig anti-vGlut2 (1:1000; catalog #AB2251, Millipore), rabbit anti-PSD95 (1:500; catalog

#51-6900, Invitrogen), mouse anti-NeuN (1:1000; catalog #ab104224, Abcam), and rabbit anti-PACAP (1:500; catalog #bs0190-R, Bioss). The following secondary antibodies were used: goat anti-rabbit Cy3, goat anti-guinea pig Alexa Fluor 647, goat anti-rabbit Dylight 405, and goat anti-mouse Cy3 (1:500; Jackson ImmunoResearch).

Electrophysiology and biocytin cell filling

Electrophysiological recordings were performed in animals at 5–6 weeks post-surgery. Coronal sections (300 μm) were prepared using a Leica VT1000 S vibratome and maintained in oxygenated (95% O_2/5% CO_2) aCSF containing the following (in mM): 26 NaHCO3, 126 NaCl, 2.5 KCl, 1.25 NaH_2PO_4, 1 $MgSO_4$, 2 CaCl2, and 10 D-glucose at 32°C for 1 h before recording. Whole-cell recordings were performed at 33°C using a Nikon Eclipse FN1 microscope, a MultiClamp 700B amplifier (Molecular Devices), Digidata 1440 A Digitizer (Molecular Devices), pClampex 10.2 program software (Molecular Devices) and sampled at 10 kHz. For voltage-clamp recordings, a cesium-based internal solution was used containing the following (in mM): 120 D-gluconic acid, 10 HEPES, 0.5 CaCl2, 20 TEA-Cl, 120 CsOH, 10 EGTA, 2 ATP, and 0.3 GTP, with a final osmolality between 295–300 mOsm. For biocytin filling experiments, 1% biocytin was dissolved into the internal solution. sEPSC experiments were performed under whole-cell conditions in slices submerged in aCSF containing 10 μM SR 95531 (catalog #1262, Tocris Bioscience). Neurons were held at −60 mV and recorded for 3 min. Access resistance was monitored before and after recordings, and neurons with a >25% change in access were excluded. Analysis was performed using MATLAB and Clampfit (Molecular Devices) software, and sEPSC recordings were analyzed using the MiniAnalysis program (Synaptosoft).

For biocytin cell filling and streptavidin/immunofluorescent labeling, neurons were patched for 5 min to allow biocytin internal solution to fill the cell while sEPSCs were recorded. Cell membranes were resealed, and slices were kept in aCSF for 45 min to 1 h to allow biocytin to diffuse through the neuron. Slices were fixed in 4% paraformaldehyde overnight at 4°C and washed in 1× PBS before permeabilization with 0.5% Triton X-100 for 3–4 h at room temperature. Slices were blocked for 2 h at room temperature in 1% BSA, 0.5% NGS, and 0.4% Triton X-100 in 1× PBS and incubated in primary antibody (anti-PACAP and/or anti-GFP as previously described) overnight at 4°C. The following day, slices were incubated in streptavidin-Cy3 (1:50; catalog #434315, Invitrogen) or streptavidin-DyLight 405 (1:500; catalog #016-470-084, Jackson ImmunoResearch) and previously described secondary antibodies overnight at 4°C. After successive washes in PBS/glycerol solution, slices were mounted and coverslipped using Fluoromount G (Southern Biotech). Images were acquired with a Nikon A1R confocal microscope at 40× magnification. The proximity of biocytin-filled cells to tdTomato or GFP expression and correct viral targeting were confirmed. Biocytin-filled neurons were reconstructed with Imaris software to assess for positive PACAP staining, and only those $PACAP^+$ cells were included in analyses.

Statistical analysis

GraphPad Prism 9 software was used to perform all statistical analyses. All values are depicted as mean ± SEM. Comparisons were determined to be statistically significant when $p < 0.05$. Two-tailed unpaired *t* tests were used for comparisons of two groups, including Western blot data, area under the curve data for glucose/insulin tolerance tests, serum insulin and glucagon levels, tissue NE content, adipocyte size, gonadal white adipose tissue (gWAT) triglyceride content, number of c-fos^+ cells, average sEPSC frequency and amplitude, and excitatory synapse number. Two-way repeated-measures ANOVA with Bonferroni's multiple comparisons were performed to analyze weekly body weight and food intake measurements, as well as time course data for glucose and insulin tolerance tests. Two-way ANOVA, with Tukey's or Bonferroni's multiple comparisons test, respectively, was performed for comparisons of serum-free fatty acid and glycerol levels in fed and fasted animals and percentages of triglyceride types in gWAT. Nested *t* tests were performed to compare the number of excitatory presynaptic puncta per $PACAP^+$ cell between control and mutant mice. Kolmogorov–Smirnov tests were used to analyze adipocyte size distributions and distributions from electrophysiological data. Statistics used for each dataset are indicated in the figure legends. Number (*n*) for each dataset is indicated in the figure legends.

Results

Astrocytic mGluR5 in adult VMH is not required for feeding or body weight regulation

Because expression of mGluR5 in astrocytes is developmentally regulated and thought to be very low to absent in the mature brain (Cai et al., 2000; Sun et al., 2013; Morel et al., 2014), its function and relevance in adult animals has been highly debated. As a first step toward examining the role of astrocytic mGluR5 in adult VMH, we sought to confirm its expression there. Consistent with previous observations (Van Den Pol et al., 1995), immunolabeling studies revealed mGluR5 expression in astrocytes selectively labeled by delivery of AAV5-GFAP-eGFP, whose serotype and promoter combination confers astrocyte-specific viral transduction, into the VMH of adult wild-type mice (Fig. 1*A*).

To interrogate the role of astrocytic mGluR5 in the VMH, wegenerated mutant ($mGluR5^{GFAP\text{-}Cre}$) and control ($mGluR5^{GFAP\text{-}GFP}$) mice by bilateral stereotaxic delivery of AAV5-GFAP-eGFP-Cre and AAV5-GFAP-eGFP, respectively, into the VMH of 8- to 12-week-old floxed mGluR5 mice (Fig. 1*B*). Control experiments we reported previously demonstrated that injection of these viruses in the VMH of wild-type C57BL/6 mice did not produce nonspecific effects (Ameroso et al., 2022). Mice receiving AAV5-GFAP-eGFP-Cre exhibited astrocyte-specific expression of GFP in the VMH as indicated by its colocalization with the astrocyte-specific marker Sox9 but not with neuronal NeuN (Fig. 1*C*,*D*). We chose to use Sox9 to label astrocytes within the VMH (Sun et al., 2017) as this transcription factor localizes primarily to the nucleus, as it is the case with eGFP-Cre expression driven by AAV5-GFAP-eGFP-Cre. RNAscope analysis showed depletion of Grm5 transcripts in VMH astrocytes, marked by Sox9 mRNA expression, in $mGluR5^{GFAP\text{-}Cre}$ mice (Fig. 1*E*). Furthermore, female and male $mGluR5^{GFAP\text{-}Cre}$ mutant mice exhibited a 65.8 and 42.5% decrease, respectively, in mGluR5 protein expression in the VMH (Fig. 1*F*–*H*), reflecting that neuronal mGluR5 expression persists following depletion in astrocytes.

Neither female nor male $mGluR5^{GFAP\text{-}Cre}$ mutant mice fed a chow diet exhibited significant differences in overall body weight when monitored for 14 weeks post-surgery (Fig. 2*A*–*D*). Consistent with these observations, chow intake was similar in mutants compared with controls (Fig. 2*E*,*F*). Body weight gain of mutants was also comparable to that of controls when challenged with a high fat diet (Fig. 2*G*,*H*). These results indicate that mGluR5 is not required in VMH astrocytes during adulthood for the regulation of body weight or feeding.

Selective deletion of astrocytic mGluR5 in the VMH enhances glucose tolerance

The VMH contains neuronal subpopulations that facilitate glucose balance by promoting glucose production or utilization in response to peripheral glycemic status signals (Kang et al., 2004; Shimazu and Minokoshi, 2017; Tu et al., 2022). To test whether astrocytic mGluR5 mediates these actions, we performed GTTs in $mGluR5^{GFAP\text{-}Cre}$ and $mGluR5^{GFAP\text{-}GFP}$ mice fed a chow diet at 9 weeks post-surgery. Fasting levels of glucose were not significantly altered in mutant mice compared with controls (Fig. 3*A*, *C*, time point 0). However, $mGluR5^{GFAP\text{-}Cre}$ male and female mice exhibited significantly enhanced glucose tolerance (Fig.

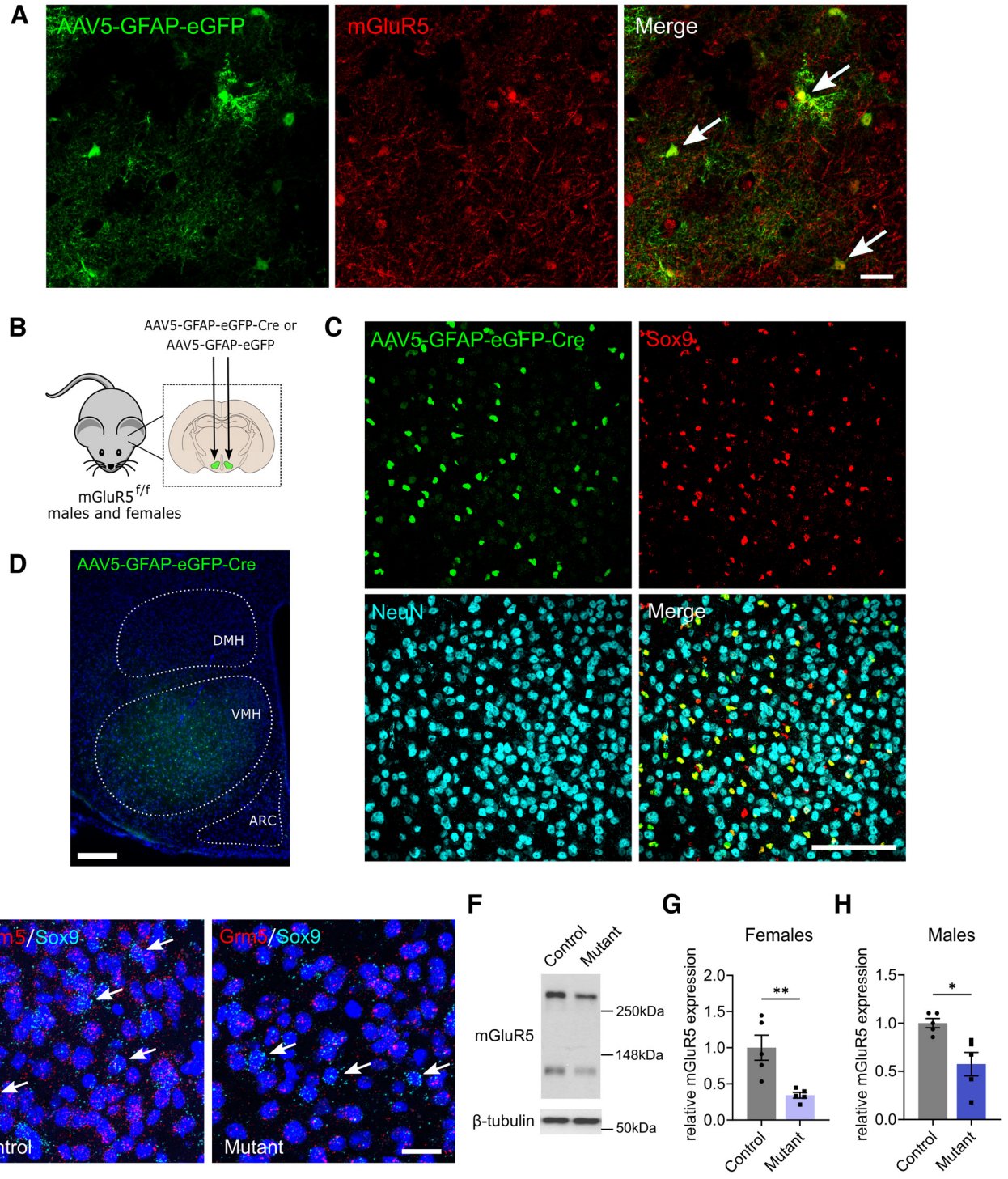

Figure 1. Selective depletion of mGluR5 in VMH astrocytes in adult mice. ***A***, Expression of mGluR5 (red) in adult mouse VMH astrocytes labeled with AAV5-GFAP-eGFP (green). White arrows indicate colocalization of GFP and mGluR5. Scale bar, 25 μm. ***B***, Diagram showing experimental approach for virally mediated bilateral depletion of mGluR5 in VMH astrocytes. ***C***, Coimmunolabeling studies indicating that AAV5-GFAP-eGFP-Cre (GFP^+, green) specifically transduces astrocytes ($Sox9^+$, red) and is excluded from neurons ($NeuN^+$, cyan). Scale bar, 50 μm. ***D***, Representative image showing viral spread (AAV5-GFAP-eGFP-Cre, green) within the VMH (DAPI, blue). DMH, Dorsomedial hypothalamus; ARC, arcuate nucleus. Scale bar, 200 μm. ***E***, Representative images of RNAscope staining showing expression of Grm5 transcripts (red) in astrocytes marked by Sox9 mRNA expression (cyan) in $mGluR5^{GFAP\text{-}GFP}$ control and $mGluR5^{GFAP\text{-}Cre}$ mutant mice. White arrows indicate astrocytes containing Grm5 mRNA in a control animal and astrocytes lacking Grm5 in a mutant mouse. Scale bar, 50 μm. ***F***, Representative Western blot of VMH mGluR5 protein expression with β-tubulin loading control in male $mGluR5^{GFAP\text{-}GFP}$ control and $mGluR5^{GFAP\text{-}Cre}$ mutant mice. ***G***, Quantification of VMH mGluR5 protein expression in female $mGluR5^{GFAP\text{-}GFP}$ controls ($n = 5$) and $mGluR5^{GFAP\text{-}Cre}$ mutants ($n = 5$). Unpaired t test, $t_{(8)} = 3.697$, $^{**}p = 0.006$. ***H***, Quantification of VMH mGluR5 protein expression in male $mGluR5^{GFAP\text{-}GFP}$ controls ($n = 5$) and $mGluR5^{GFAP\text{-}Cre}$ mutants ($n = 5$). Unpaired t test, $t_{(8)} = 3.250$, $^{*}p = 0.012$.

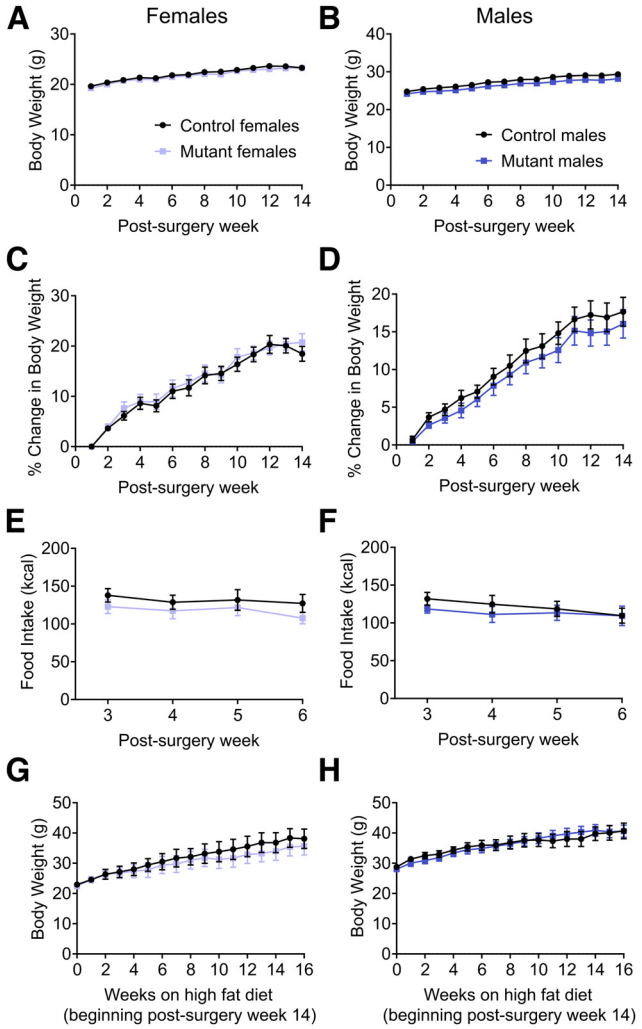

Figure 2. mGluR5 is not required in VMH astrocytes for regulation of body weight or feeding. ***A***, Body weights of female mGluR5$^{GFAP\text{-}GFP}$ controls ($n = 14$) and mGluR5$^{GFAP\text{-}Cre}$ mutants ($n = 12$) fed standard chow. Two-way repeated-measures ANOVA, Time, $F_{(3.757,90.16)} = 131.9$, $^{****}p < 0.0001$; Genotype, $F_{(1,24)} = 0.3675$, $p = 0.55$; Interaction, $F_{(13,312)} = 0.5074$, $p = 0.92$. Bonferroni multiple comparisons, no significance. ***B***, Body weights of male mGluR5$^{GFAP\text{-}GFP}$ controls ($n = 13$) and mGluR5$^{GFAP\text{-}Cre}$ mutants ($n = 12$) fed standard chow. Two-way repeated-measures ANOVA, Time, $F_{(1.684,38.74)} = 102.4$, $^{****}p < 0.0001$; Genotype, $F_{(1,23)} = 2.251$, $p = 0.15$; Interaction, $F_{(13,299)} = 0.5444$, $p = 0.90$. Bonferroni multiple comparisons, no significance. ***C***, Percentage body weight gain in female controls ($n = 14$) and mutants ($n = 12$) fed standard chow. Two-way repeated-measures ANOVA, Time, $F_{(13,312)} = 0.5237$, $p < 0.0001$; Genotype, $F_{(1,24)} = 0.1318$, $p = 0.72$; Interaction, $F_{(13,312)} = 0.5237$, $p = 0.91$. Bonferroni multiple comparisons, no significance. ***D***, Percentage body weight gain in male controls ($n = 13$) and mutants ($n = 12$) fed standard chow. Two-way repeated-measures ANOVA, Time, $F_{(1.991,45.79)} = 123.1$, $p < 0.0001$; Genotype, $F_{(1,23)} = 0.7029$, $p = 0.41$; Interaction, $F_{(13,299)} = 0.3044$, $p = 0.99$. Bonferroni multiple comparisons, no significance. ***E***, Food intake of female controls ($n = 16$) and mutants ($n = 13$) fed standard chow. Two-way repeated-measures ANOVA, Time, $F_{(2.368,63.95)} = 1.679$, $p = 0.19$; Genotype, $F_{(1,27)} = 1.124$, $p = 0.30$; Interaction, $F_{(3,81)} = 0.2539$, $p = 0.86$. Bonferroni multiple comparisons, no significance. ***F***, Food intake of male controls ($n = 17$) and mutants ($n = 13$) fed standard chow. Two-way repeated-measures ANOVA, Time, $F_{(1.611,45.11)} = 3.013$, $p = 0.070$; Genotype, $F_{(1,28)} = 0.3838$, $p = 0.54$; Interaction, $F_{(3,84)} = 0.7811$, $p = 0.51$. Bonferroni multiple comparisons, no significance. ***G***, Body weights of female controls ($n = 6$) and mutants ($n = 6$) fed a high fat diet. Two-way repeated-measures ANOVA, Time, $F_{(16,160)} = 36.03$, $^{****}p < 0.0001$; Genotype, $F_{(1,10)} = 0.2355$, $p = 0.64$; Interaction, $F_{(16,160)} = 0.6521$, $p = 0.84$. Bonferroni multiple comparisons, no significance. ***H***, Body weights of male controls ($n = 5$) and mutants ($n = 6$) fed a high-fat diet. Two-way repeated-measures ANOVA, Time, $F_{(16,144)} = 49.64$, $^{****}p < 0.0001$; Genotype, $F_{(1,9)} = 0.001333$, $p = 0.97$; Interaction, $F_{(16,144)} = 1.313$, $p = 0.20$. Bonferroni multiple comparisons, no significance.

3*A–D*). This is in contrast to our previously reported effects of depleting mGluR5 in VMH SF1^{+} neurons, which results in glucose intolerance only in mutant females (Fagan et al., 2020). ITTs suggest that alterations in insulin sensitivity do not significantly contribute to the observed changes in glucose tolerance. Accordingly, female mGluR5$^{GFAP\text{-}Cre}$ mutant mice only exhibited a mild but significant reduction in glucose levels at the 120 min time point following insulin administration (Fig. 3*E*), whereas male mutants displayed responses similar to those of mGluR5$^{GFAP\text{-}GFP}$ controls (Fig. 3*G*). Furthermore, serum glucagon content in mice with insulin-induced hypoglycemia was not significantly altered in mGluR5$^{GFAP\text{-}Cre}$ mutants compared with their sex-matched controls (Fig. 3*K*,*L*), suggesting that the counter-regulatory response to hypoglycemia was not altered.

We hypothesized that enhanced glucose tolerance in mGluR5$^{GFAP\text{-}Cre}$ mutant mice could result from increased levels of circulating insulin in response to acute hyperglycemia. To test this, glucose-stimulated insulin secretion was measured in mutant and control mice. At baseline, fasted serum levels of insulin in mutant females and males were similar to controls. However, insulin levels were significantly increased in female mutants by 36% and trended toward a significant increase of 42% in mutant males following administration of a glucose bolus compared with their respective controls (Fig. 3*I*,*J*).

The VMH facilitates glycemic balance via regulation of sympathetic output to metabolic organs in the periphery involved in glucose mobilization and production (Shimazu et al., 1991; Minokoshi et al., 1994; Haque et al., 1999; Liu et al., 2013). To investigate whether changes in sympathetic tone might contribute to enhanced glucose tolerance in mGluR5$^{GFAP\text{-}Cre}$ mice, norepinephrine (NE) content was measured in brown adipose tissue (BAT), liver, and skeletal muscle and found to be comparable to that of sex-matched controls (Fig. 4). The results suggest that astrocytic mGluR5 in the VMH influences peripheral glucose homeostasis via regulation of insulin secretion during acute hyperglycemia independently of body weight.

mGluR5 in VMH astrocytes regulates adipocyte size and sympathetic tone in gonadal white adipose tissue

The VMH regulates peripheral lipid balance through efferent projections to autonomic brain regions that regulate sympathetic output to fat depots (Kumon et al., 1976; Takahashi and Shimazu, 1981, 1982; Saito et al., 1989; Lindberg et al., 2013). We previously reported that depletion of mGluR5 from VMH SF1^{+} neurons dysregulates lipid homeostasis in female mice despite exhibiting normal body weights (Fagan et al., 2020). Therefore, we investigated whether astrocytic mGluR5 in the VMH might also influence lipid balance. The size of adipocytes in gWAT was significantly reduced in female and male mGluR5$^{GFAP\text{-}Cre}$ mice by 47.9 and 40.6%, respectively, compared with controls (Fig. 5*A–C*). The relative frequency distributions corroborated the alterations in gWAT cell size, with higher percentages of adipocytes comprising smaller cell sizes in female and male mutant mice relative to their respective controls (Fig. 5*D*,*E*).

As reduced white adipocyte size may result from elevated lipolysis (Stenkula and Erlanson-Albertsson, 2018), we measured levels of serum glycerol and fFFAs, the end products of lipolysis, in both fed and fasted mice. Control mGluR5$^{GFAP\text{-}GFP}$ mice exhibited significantly increased levels of FFAs and glycerol in the fasted state compared with fed state, as expected. In contrast, feeding status had no significant effect on levels of FFA and glycerol in mutant females, and fasted male mutants only experienced a significant increase in glycerol compared with fed male

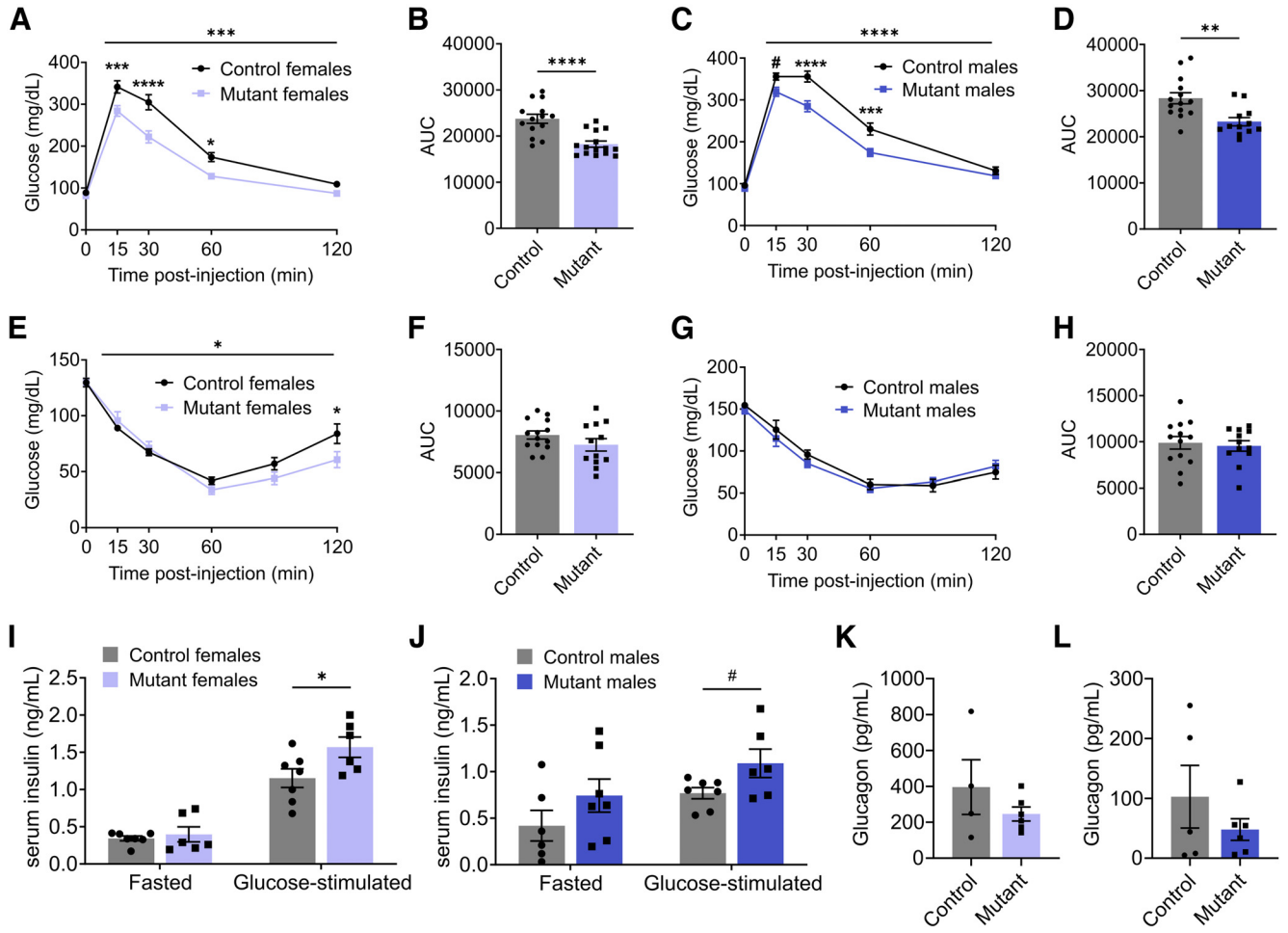

Figure 3. Depletion of astrocytic mGluR5 in the VMH enhances glucose tolerance in both female and male mice. ***A***, Glucose tolerance test in female mGluR5$^{GFAP\text{-}GFP}$ controls ($n = 14$) and mGluR5$^{GFAP\text{-}Cre}$ mutants ($n = 15$). Two-way repeated-measures ANOVA, Time, $F_{(4,108)} = 272.0$, ****$p < 0.0001$; Genotype, $F_{(1,27)} = 19.53$, ***$p = 0.0001$; Interaction, $F_{(4,108)} = 5.797$, ***$p = 0.0003$. Bonferroni's multiple comparisons, ***$p = 0.0007$ at 15 min, ****$p < 0.0001$ at 30 min, *$p = 0.012$ at 60 min. ***B***, GTT area under the curve for female control and mutant mice. Unpaired *t* test, $t_{(27)} = 4.697$, ****$p < 0.0001$. ***C***, Glucose tolerance test in male mGluR5$^{GFAP\text{-}GFP}$ controls ($n = 14$) and mGluR5$^{GFAP\text{-}Cre}$ mutants ($n = 12$). Two-way repeated-measures ANOVA, Time, $F_{(4,96)} = 455.4$, ****$p < 0.0001$; Genotype, $F_{(1,24)} = 11.67$, **$p = 0.0023$; Interaction, $F_{(4,96)} = 6.893$, ****$p < 0.0001$. Bonferroni's multiple comparisons, #$p = 0.058$ at 15 min, ****$p < 0.0001$ at 30 min, ***$p = 0.0007$ at 60 min. ***D***, GTT area under the curve for male control and mutant mice. Unpaired *t* test, $t_{(24)} = 3.327$, **$p = 0.0028$. ***E***, Insulin tolerance test of female controls ($n = 14$) and mutants ($n = 12$). Two-way repeated-measures ANOVA, Time, $F_{(5,120)} = 94.32$, ****$p < 0.0001$; Genotype, $F_{(1,24)} = 1.507$, $p = 0.23$; Interaction, $F_{(5,120)} = 2.879$, *$p = 0.017$. Bonferroni's multiple comparisons, *$p = 0.016$ at 120 min. ***F***, ITT area under the curve for female control and mutant mice. Unpaired *t* test, $t_{(24)} = 1.358$, $p = 0.19$. ***G***, Insulin tolerance test of male controls ($n = 13$) and mutants ($n = 12$). Two-way repeated-measures ANOVA, Time, $F_{(5,115)} = 103.5$, ****$p < 0.0001$; Genotype, $F_{(1,23)} = 0.2145$, $p = 0.65$; Interaction, $F_{(5,115)} = 1.104$, $p = 0.36$; Bonferroni's multiple comparisons. ***H***, ITT area under the curve for males. Unpaired *t* test, $t_{(23)} = 0.3781$, $p = 0.71$. ***I***, Serum insulin levels in fasted ($n = 6$–7 mice/group) and glucose-stimulated ($n = 6$-7 mice/group) control and mutant female mice. Unpaired *t* test, Fasted, $t_{(11)} = 0.5483$, $p = 0.59$; Glucose-stimulated, $t_{(11)} = 2.249$, *$p = 0.046$. ***J***, Serum insulin levels in fasted ($n = 6$–7 mice/group) and glucose-stimulated ($n = 6$–7 mice/group) control and mutant male mice. Unpaired *t* test, Fasted, $t_{(11)} = 1.319$, $p = 0.21$; Glucose-stimulated, $t_{(11)} = 2.071$, #$p = 0.063$. ***K***, Serum glucagon levels in female control ($n = 4$) and mutant ($n = 6$) mice with insulin-induced hypoglycemia. Unpaired *t* test, $t_{(8)} = 1.152$, $p = 0.28$. ***L***, Serum glucagon levels in male control ($n = 5$) and mutant ($n = 6$) mice with insulin-induced hypoglycemia. Unpaired *t* test, $t_{(9)} = 1.1067$, $p = 0.31$.

mutants. However, levels of circulating glycerol and FFAs were not significantly different between mutants and controls in the fed or fasted conditions (Fig. 5*F*,*I*). We also measured the triglyceride content of gWAT and found comparable levels of total triglyceride content as well as the percentage of various triglyceride subtypes in mutants and controls of both sexes (Fig. 6). These data suggest that reduced adipocyte size is not associated with altered lipid mobilization from gonadal white adipose tissue.

Because the size, number, and function of white adipocytes is greatly influenced by the sympathetic innervation to this tissue (Ramseyer and Granneman, 2016; Ryu and Buettner, 2019), NE content was measured in gWAT and iWAT as well as in serum of mGluR5$^{GFAP\text{-}Cre}$ and mGluR5$^{GFAP\text{-}GFP}$ mice fed a chow diet. Circulating levels of norepinephrine were comparable between mutants and their sex-matched controls (Fig. 7*A*,*D*). However, NE levels were significantly elevated in gWAT of both female and male mutant mice by nearly threefold in comparison with their respective controls (Fig. 7*B*,*E*), indicating increased sympathetic tone in this adipose tissue depot. In comparison, NE content was similar in iWAT of mutants and controls (Fig. 7*C*,*F*). Overall, the results show that astrocytic mGluR5 influences both adipocyte size and sympathetic tone in gonadal white adipose tissue.

Astrocytic mGluR5 modulates VMH neuronal activity during acute hyperglycemia

Changes in peripheral glucose levels induce alterations in VMH neuronal activity that subsequently drive the appropriate physiological responses to achieve euglycemia (Dunn-Meynell et al., 1997; Routh et al., 2014; Wu et al., 2014; Shimazu and

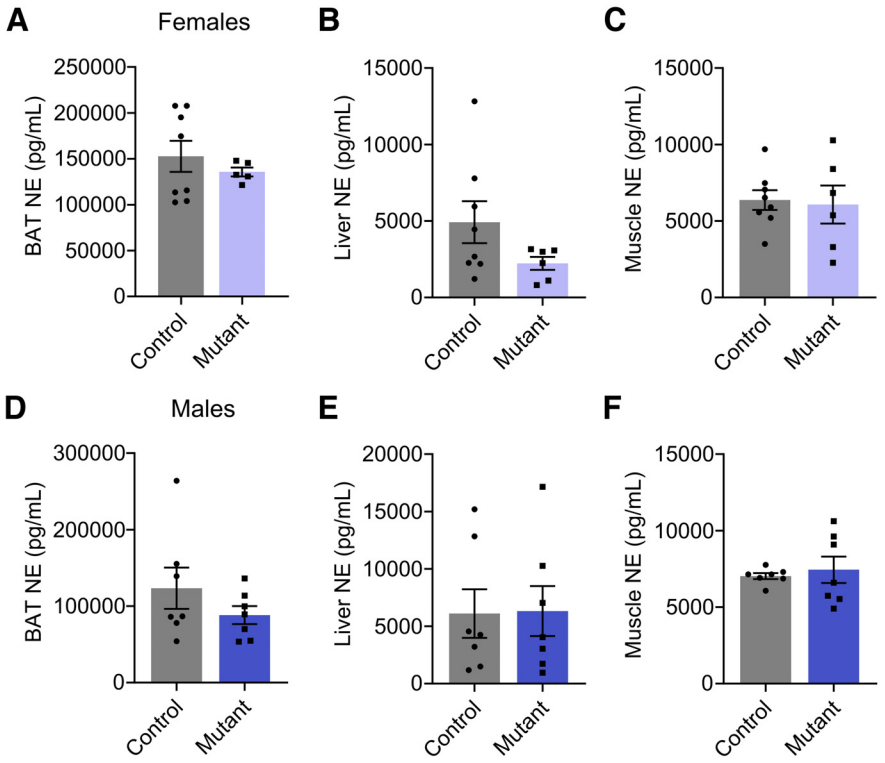

Figure 4. mGluR5 depletion in VMH astrocytes does not affect sympathetic tone in brown adipose tissue, liver, and skeletal muscle. ***A***, BAT norepinephrine levels in female mGluR5$^{GFAP\text{-}GFP}$ controls ($n = 8$) and mGluR5$^{GFAP\text{-}Cre}$ mutants ($n = 5$). Unpaired t test, $t_{(11)} = 0.7650$, $p = 0.46$. ***B***, Liver norepinephrine levels in female controls ($n = 8$) and mutants ($n = 6$). Unpaired t test, $t_{(12)} = 1.638$, $p = 0.13$. ***C***, Skeletal muscle norepinephrine levels in female controls ($n = 8$) and mutants ($n = 6$). Unpaired t test, $t_{(12)} = 0.2236$, $p = 0.83$. ***D***, BAT norepinephrine levels in male mGluR5$^{GFAP\text{-}GFP}$ controls ($n = 7$) and mGluR5$^{GFAP\text{-}Cre}$ mutants ($n = 7$). Unpaired t test, $t_{(12)} = 1.193$, $p = 0.26$. ***E***, Liver norepinephrine levels in male controls ($n = 7$) and mutants ($n = 7$). Unpaired t test, $t_{(12)} = 0.07{,}228$, $p = 0.94$. ***F***, Skeletal muscle norepinephrine levels in male controls ($n = 7$) and mutants ($n = 7$). Unpaired t test, $t_{(12)} = 0.4693$, $p = 0.65$.

Minokoshi, 2017). As a single astrocyte can simultaneously contact thousands of synapses in the rodent brain and broadly influence neuronal activity (Bushong et al., 2002; Halassa et al., 2007; Araque et al., 2014), we asked whether astrocytic mGluR5 has an impact on VMH neuronal activity during states of acute hyperglycemia. c-fos expression was used as a surrogate marker of VMH neuronal activity 60 min following delivery of a glucose bolus in fasted mice. At this time point, levels of circulating glucose are falling from the peak level following glucose administration as shown in Figure 3, *A* and *C*. Control mGluR5$^{GFAP\text{-}GFP}$ mice exhibited a high density of c-fos^{+} cells primarily in the central region of the VMH (Fig. 8*A*). This response was blunted in mGluR5$^{GFAP\text{-}Cre}$ mutants and significantly reduced by 33.2 and 24.5% in female and male mice, respectively (Fig. 8*B*,*C*).

Considering the improved glucose tolerance observed in mGluR5$^{GFAP\text{-}Cre}$ mice, we hypothesized that PACAP-expressing neurons in the VMH (PACAP^{VMH}) were the subpopulation of cells exhibiting reduced activity during acute hyperglycemia in mutant mice. PACAP^{+} cells are found throughout the VMH, and a subset of them in the central VMH are intrinsically glucose sensing (Hawke et al., 2009; Khodai et al., 2018). Notably, chemogenetic activation of PACAP^{VMH} neurons increased blood glucose levels while inhibiting insulin secretion and without affecting levels of the counterregulatory hormone glucagon (Khodai et al., 2018). Coimmunolabelling for PACAP and c-fos in glucose-challenged mice revealed that the vast majority of activated cells at 60 min after glucose administration were PACAP-containing (Fig. 8*D*). Importantly, the number of c-fos^{+}/PACAP^{+} cells in female and male mutants was significantly reduced by 34.2 and 24.9%, respectively. In contrast, the numbers of c-fos^{+}/PACAP^{-} cells were not significantly different between mutants and controls in either sex (Fig. 8*E*, *F*). Overall, the results suggest that depletion of astrocytic mGluR5 diminishes the activity of PACAP^{VMH} cells in response to a glucose challenge.

Depletion of astrocytic mGluR5 decreases the excitatory drive onto VMH PACAP^{+} neurons

mGluR5 plays a key role in astrocytic regulation of excitatory synaptic activity, acting as glutamate sensor in other brain regions (Panatier et al., 2011). We investigated the role of astrocytic mGluR5 in regulating excitatory drive in the VMH. For this, whole-cell recordings were performed in the dorsomedial and central subregions of the VMH (dm/cVMH), where there is an abundance of glucose-regulating neuronal subpopulations (Garfield et al., 2014; Meek et al., 2016; Stanley et al., 2016; Toda et al., 2016; Khodai et al., 2018) and where we observed glucose-induced c-fos expression (Fig. 8). Recordings of sEPSCs were performed in the presence of gabazine to isolate excitatory events (Fig. 9*A*–*C*). Frequency of sEPSCs was significantly decreased in both female and male mGluR5$^{GFAP\text{-}Cre}$ mice compared with their sex-matched controls by 25.3 and 41.9%, respectively (Fig. 9*D*,*H*). This was accompanied by a rightward shift in the distribution of interevent interval for both sexes (Fig. 9*E*,*I*). Furthermore, male mutant mice exhibited a trend toward decreased sEPSC amplitude and a leftward shift in the distribution of event amplitude compared with male controls (Fig. 9*J*,*K*). sEPSC amplitude was similar in female mutants and controls (Fig. 9*F*,*G*).

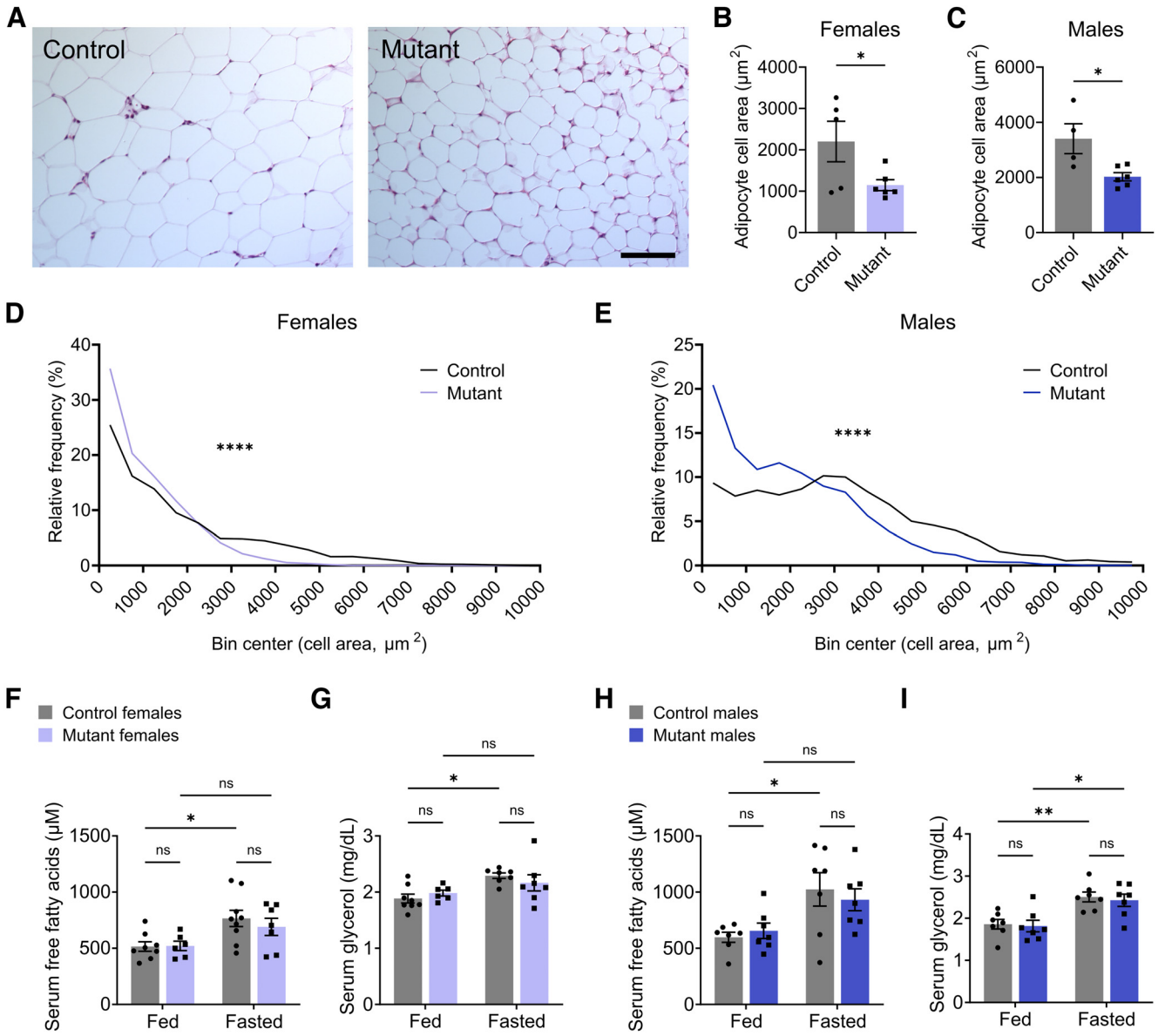

Figure 5. Astrocytic mGluR5 in the VMH regulates adipocyte size in gonadal white adipose tissue without affecting lipolysis. ***A***, Representative image of hematoxylin and eosin staining of gWAT adipocytes in female mGluR5$^{GFAP\text{-}GFP}$ controls and mGluR5$^{GFAP\text{-}Cre}$ mutants. Scale bar, 100 μm. ***B***, Quantification of gWAT adipocyte size in female controls ($n = 5$) and mutants ($n = 6$). Unpaired t test, $t_{(9)} = 2.269$, $^*p = 0.049$. ***C***, Quantification of gWAT adipocyte size in male mGluR5$^{GFAP\text{-}GFP}$ controls ($n = 4$) and mGluR5$^{GFAP\text{-}Cre}$ mutants ($n = 6$). Unpaired t test, $t_{(8)} = 2.950$, $^*p = 0.018$. ***D***, Relative frequency distributions of gWAT adipocyte sizes from female controls ($n = 4287$ cells from 5 mice) and mutants ($n = 8353$ cells from 6 mice). Kolmogorov–Smirnov test, $^{****}p < 0.0001$. ***E***, Relative frequency distributions of gWAT adipocyte sizes from male controls ($n = 2220$ cells from 4 mice) and mutants ($n = 5412$ cells from 6 mice). Kolmogorov–Smirnov test, $^{****}p < 0.0001$. ***F***, Serum free fatty acid levels in fed ($n = 6$–8 mice/group) and fasted ($n = 7$–9 mice/group) control and mutant females. Two-way ANOVA, Energy status, $F_{(1,26)} = 10.78$, $^{**}p = 0.0029$; Genotype, $F_{(1,26)} = 0.2987$, $p = 0.59$; Interaction, $F_{(1,26)} = 0.3953$, $p = 0.54$. Tukey's multiple comparisons, $^*p = 0.030$ for fed controls versus fasted controls. ***G***, Serum glycerol levels in fed ($n = 6$–8 mice/group) and fasted ($n = 7$ mice/group) control and mutant females. Two-way ANOVA, Energy status, $F_{(1,24)} = 10.26$, $^{**}p = 0.0038$; Genotype, $F_{(1,24)} = 0.02{,}375$, $p = 0.88$; Interaction, $F_{(1,24)} = 1.504$, $p = 0.23$. Tukey's multiple comparisons, $^*p = 0.017$ for fed controls versus fasted controls. ***H***, Serum-free fatty acid levels in fed ($n = 7$ mice/group) and fasted ($n = 7$ mice/group) control and mutant males. Two-way ANOVA, Energy status, $F_{(1,24)} = 12.79$, $^{**}p = 0.0015$; Genotype, $F_{(1,24)} = 0.03{,}181$, $p = 0.86$; Interaction, $F_{(1,24)} = 0.5854$, $p = 0.45$. Tukey's multiple comparisons, $^*p = 0.025$ for fed controls versus fasted controls. ***I***, Serum glycerol levels in fed ($n = 7$ mice/group) and fasted ($n = 7$ mice/group) control and mutant males. Two-way ANOVA, Energy status, $F_{(1,24)} = 0.5854$, $^{****}p < 0.0001$; Genotype, $F_{(1,24)} = 0.2087$, $p = 0.65$; Interaction, $F_{(1,24)} = 0.01{,}816$, $p = 0.89$. Tukey's multiple comparisons, $^{**}p = 0.0083$ for fed controls versus fasted controls; $^*p = 0.013$ for fed mutants versus fasted mutants. ns = no significance.

Because active VMH neurons during a glucose challenge are largely PACAP$^+$ (Fig. 8*D*), we asked whether excitatory transmission was affected specifically in these cells in mGluR5$^{GFAP\text{-}Cre}$ mice. Cells were filled with biocytin during whole-cell sEPSC recordings and *post hoc* immunostaining with anti-PACAP performed to identify recorded cells that were also PACAP$^+$ (Fig. 10*A*). sEPSC frequency in mutant PACAP$^+$ cells was significantly reduced in both female and male (by 35.5 and 45.8%, respectively) mutant mice compared with sex-matched controls. This was also reflected in a significant rightward shift in the distributions of interevent interval (Fig. 10*D*,*E*,*H*,*I*). Average sEPSC amplitudes and amplitude distributions in PACAP^{VMH} cells were similar between mutants and controls in both sexes (Fig. 10*F*,*G*,*J*,*K*). These results indicate that astrocytic mGluR5 is an essential player mediating excitatory neurotransmission onto PACAP$^+$ neurons in the VMH.

mGluR5 depletion in astrocytes disrupts VMH excitatory synaptic physiology

Astrocytes actively participate in the regulation of synaptogenesis, synaptic stability, and plasticity, and mGluR5 mediates some

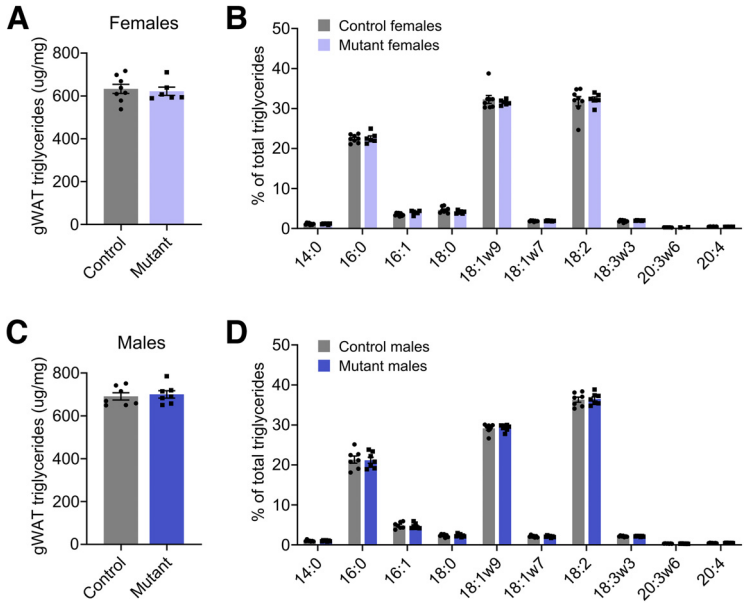

Figure 6. Depletion of mGluR5 in VMH astrocytes does not alter triglyceride content in gonadal white adipose tissue. ***A***, Total triglyceride content in gonadal WAT of female mGluR5$^{GFAP\text{-}GFP}$ control ($n = 8$) and mGluR5$^{GFAP\text{-}Cre}$ mutant ($n = 6$) mice. Unpaired *t* test, $t_{(12)} = 0.3599$, $p = 0.73$. ***B***, Percentage of triglyceride types in gonadal WAT of female control ($n = 8$) and mutant ($n = 6$) mice. Two-way ANOVA, triglyceride type, $F_{(9,111)} = 1548$, $^{****}p < 0.0001$; genotype, $F_{(1,111)} = 0.0001829$, $p = 0.99$; interaction, $F_{(9,111)} = 0.3570$, $p = 0.95$. Bonferroni multiple comparisons, no significance. ***C***, Total triglyceride content in gonadal WAT of male mGluR5$^{GFAP\text{-}GFP}$ control ($n = 7$) and mGluR5$^{GFAP\text{-}Cre}$ mutant ($n = 7$) mice. Unpaired *t* test, $t_{(12)} = 0.3911$, $p = 0.70$. ***D***, Percentage of triglyceride types in gonadal WAT of female control ($n = 8$) and mutant ($n = 6$) mice. Two-way ANOVA, triglyceride type, $F_{(9,120)} = 2876$, $^{****}p < 0.0001$; genotype, $F_{(1,120)} = 7.910\text{e-}007$, $p = 0.99$; interaction, $F_{(9,120)} = 0.05{,}284$, $p > 0.99$. Bonferroni multiple comparisons, no significance.

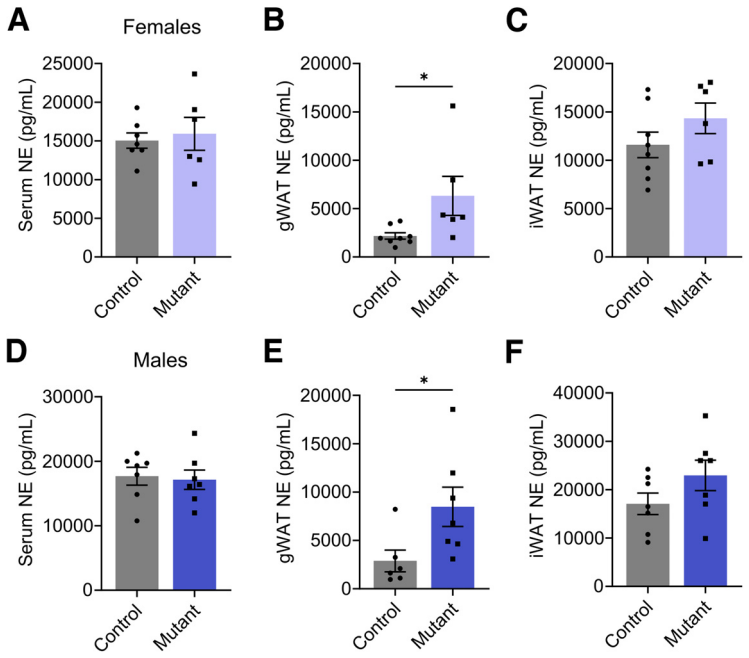

Figure 7. Astrocytic mGluR5 in the VMH regulates sympathetic output in gonadal white adipose tissue. ***A***, Serum norepinephrine levels in female mGluR5$^{GFAP\text{-}GFP}$ controls ($n = 7$) and mGluR5$^{GFAP\text{-}Cre}$ mutants ($n = 6$). Unpaired *t* test, $t_{(11)} = 0.3913$, $p = 0.70$. ***B***, gWAT norepinephrine levels in female controls ($n = 8$) and mutants ($n = 6$). Unpaired *t* test, $t_{(12)} = 2.347$, $^{*}p = 0.037$. ***C***, iWAT norepinephrine levels in female controls ($n = 8$) and mutants ($n = 6$). Unpaired *t* test, $t_{(12)} = 1.339$, $p = 0.21$. ***D***, Serum norepinephrine levels in male mGluR5$^{GFAP\text{-}GFP}$ controls ($n = 7$) and mGluR5$^{GFAP\text{-}Cre}$ mutants ($n = 7$). Unpaired *t* test, $p = 0.80$. ***E***, gWAT norepinephrine levels in male controls ($n = 6$) and mutants ($n = 7$). Unpaired *t* test, $t_{(11)} = 2.292$, $^{*}p = 0.043$. ***F***, iWAT norepinephrine levels in male controls ($n = 7$) and mutants ($n = 7$). Unpaired *t* test, $t_{(12)} = 1.530$, $p = 0.15$.

of these effects (Ullian et al., 2001; Bernardinelli et al., 2014; Chung et al., 2015; Danjo et al., 2022). To inform mechanisms underlying the reduced excitatory tone of VMH neurons in mGluR5$^{GFAP\text{-}Cre}$ mice, we measured density of excitatory synapses in this region by coimmunolabeling studies with the presynaptic and postsynaptic markers VGLUT2 and PSD95, respectively. The number of VMH excitatory synapses was significantly reduced in both female and male mutants by 26.5 and 32.5%, respectively (Fig. 11*A–C*). Examination of density of presynaptic VGLUT2 puncta onto the soma of PACAP^{VMH} cells

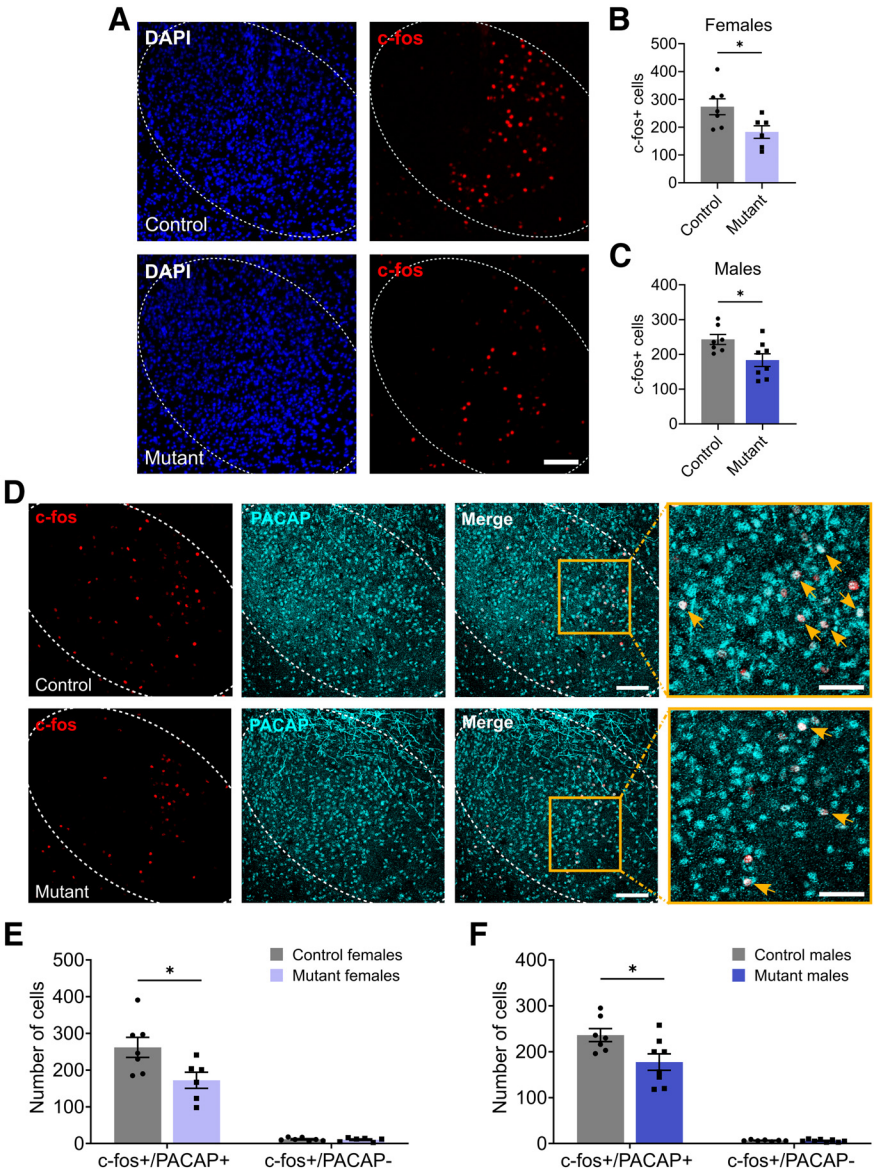

Figure 8. Astrocytic mGluR5 regulates PACAP^{+} neuronal activity in VMH during acute hyperglycemia. ***A***, Representative images of DAPI staining (blue) and immunolabeling of c-fos^{+} cells (red) in male mGluR5$^{GFAP\text{-}GFP}$ control (top) and mGluR5$^{GFAP\text{-}Cre}$ mutant (bottom) mice. Dotted line indicates VMH. Scale bar, 100 μm. ***B***, Quantification of c-fos^{+} cells in the VMH of female control ($n = 7$) and mutant ($n = 6$) mice. Unpaired *t* test, $t_{(11)} = 2.424$, $^{*}p = 0.034$. ***C***, Quantification of c-fos^{+} cells in the VMH of male control ($n = 7$) and mutant ($n = 8$) mice. Unpaired *t* test, $t_{(13)} = 2.503$, $^{*}p = 0.027$. ***D***, Representative images of coimmunolabeling studies showing colocalization of c-fos (red) and PACAP (cyan) in female control (top) and mutant (bottom) mice. Dotted line indicates VMH. Arrows point to c-fos^{+}/PACAP^{+} cells. Scale bars, low magnification, 100 μm; high magnification, 50 μm. ***E***, Quantification of c-fos^{+}/PACAP^{+} cells and c-fos^{+}/PACAP^{-} cells in the VMH of female control ($n = 7$) and mutant ($n = 6$) mice. Unpaired *t* tests, c-fos^{+}/PACAP^{+}, $t_{(11)} = 2.496$, $^{*}p = 0.030$; c-fos^{+}/PACAP^{-}, $t_{(11)} = 0.4658$, $p = 0.65$. ***F***, Quantification of c-fos^{+}/PACAP^{+} cells and c-fos^{+}/PACAP^{-} cells in the VMH of male control ($n = 7$) and mutant ($n = 8$) mice. Unpaired *t* tests, c-fos^{+}/PACAP^{+}, $t_{(13)} = 2.525$, $^{*}p = 0.025$; c-fos^{+}/PACAP^{-}, $t_{(14)} = 0.9779$, $p = 0.34$.

revealed that this synapse deficit affected this VMH neuronal subpopulation. Accordingly, female and male mGluR5$^{GFAP\text{-}Cre}$ mutants exhibited a 44.3 and 36.8% decrease, respectively, in the numbers of excitatory presynaptic puncta on PACAP^{VMH} cells (Fig. 11*D–F*), consistent with the reduced excitatory drive onto these cells revealed by the electrophysiological analysis.

Astrocytes regulate synapse formation via secretion of various synaptogenic factors, including TSP-1, TSP-2, hevin, and glypican-4 (Chung et al., 2015; Danjo et al., 2022). Thus, we sought to determine whether altered expression of those proteins in the VMH underlaid the reduced excitatory synapse density observed in mGluR5$^{GFAP\text{-}Cre}$ mutants. There were no significant differences in protein expression levels of TSP-2, hevin, or glypican-4 in mutants of either sex. mGluR5$^{GFAP\text{-}Cre}$ males displayed a trend toward a significant decrease in TSP-1 expression, whereas TSP-1 expression in mutant females was unchanged in comparison to their respective controls (Fig. 12).

In addition to regulating synapse formation, astrocytes can also promote synapse stability and function by regulating the proximity and plasticity of perisynaptic astrocyte processes (PAPs) to synapses (Bernardinelli et al., 2014). Thus, we next asked whether astrocytic mGluR5 depletion in the VMH could alter levels of ezrin, a cytoskeleton linker protein that is compartmentalized to PAPs and is required for PAP motility and plasticity in an mGluR-dependent manner (Lavialle et al., 2011). Expression levels of ezrin were significantly reduced in female and male mutants, by 30.8 and 48.1%, respectively, compared with their controls (Fig. 11*G*,*H*), suggesting that PAP formation and plasticity is impaired

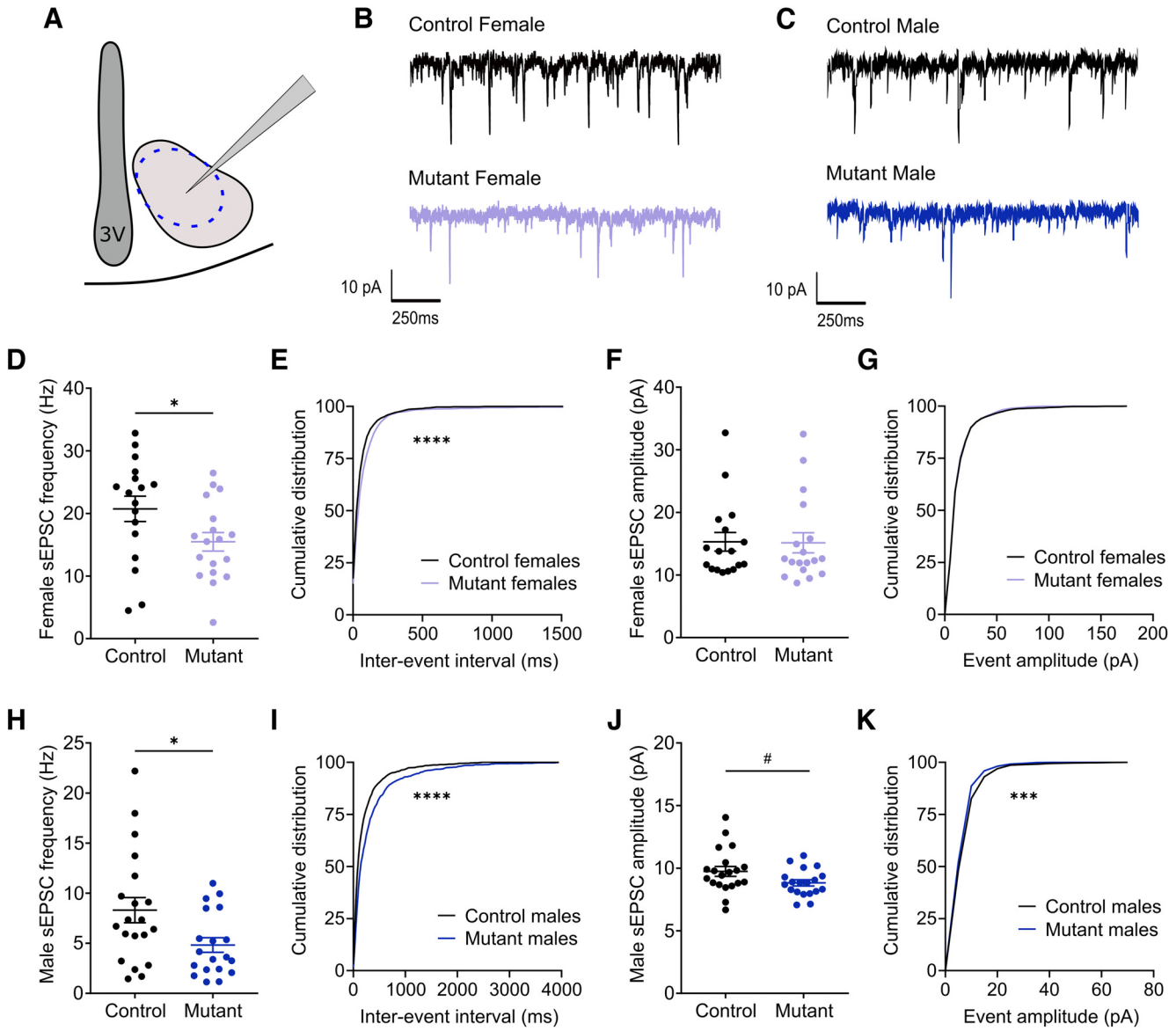

Figure 9. Excitatory tone onto dorsomedial and central VMH neurons is reduced in mGluR5$^{GFAP\text{-}Cre}$ mutant mice. ***A***, Diagram showing the dorsomedial and central VMH regions (dotted line) where whole-cell recordings were performed. ***B***, Representative traces of sEPSCs in dm/cVMH neurons from female mGluR5$^{GFAP\text{-}GFP}$ control and mGluR5$^{GFAP\text{-}Cre}$ mutant mice. ***C***, Representative traces of sEPSCs in dm/cVMH neurons from male mGluR5$^{GFAP\text{-}GFP}$ control and mGluR5$^{GFAP\text{-}Cre}$ mutant mice. ***D***, Average sEPSC frequency of VMH neurons from female controls ($n = 17$ cells from 6 animals) and mutants ($n = 18$ cells from 5 animals). Unpaired t test, $t_{(33)} = 2.122$, $^{*}p = 0.041$. ***E***, Cumulative distribution of interevent interval generated from 50 random events per recorded cell for female controls ($n = 17$ cells from 6 animals) and mutants ($n = 18$ cells from 5 animals). Kolmogorov–Smirnov test, $^{****}p < 0.0001$. ***F***, Average sEPSC amplitude of VMH neurons from female controls ($n = 17$ cells from 6 animals) and mutants ($n = 18$ cells from 5 animals). Unpaired t test, $t_{(33)} = 0.07{,}416$, $p = 0.94$. ***G***, Cumulative distribution of event amplitude generated from 50 random events per recorded cell for female controls ($n = 17$ cells from 6 animals) and mutants ($n = 18$ cells from 5 animals). Kolmogorov–Smirnov test, no significance. ***H***, Average sEPSC frequency of VMH neurons from male controls ($n = 20$ cells from 4 animals) and mutants ($n = 19$ cells from 4 animals). Unpaired t test, $t_{(37)} = 2.373$, $^{*}p = 0.023$. ***I***, Cumulative distribution of interevent interval generated from 50 random events per recorded cell for male controls ($n = 20$ cells from 4 animals) and mutants ($n = 19$ cells from 4 animals). Kolmogorov–Smirnov test, $^{****}p < 0.0001$. ***J***, Average sEPSC amplitude of VMH neurons from male controls ($n = 20$ cells from 4 animals) and mutants ($n = 19$ cells from 4 animals). Unpaired t test, $t_{(37)} = 1.936$, $\#p = 0.061$. ***K***, Cumulative distribution of event amplitude generated from 50 random events per recorded cell for male controls ($n = 20$ cells from 4 animals) and mutants ($n = 19$ cells from 4 animals). Kolmogorov–Smirnov test, $^{***}p = 0.0004$.

in these mutants. Along with ezrin, astrocyte PAPs are also enriched with the glutamate transporter, GLT-1, which mediates synaptic glutamate clearance (Danbolt et al., 1992). Because astrocytic mGluR5 regulates both astrocyte morphology and expression of GLT-1 in other brain regions during development (Morel et al., 2014), we measured GLT-1 expression in the VMH of adult mGluR5$^{GFAP\text{-}Cre}$ mutant mice. Neither female nor male mutant mice exhibited significant alterations to GLT-1 protein content in the VMH (Fig. 11*I*,*J*). Collectively, the results indicate that mGluR5 is a key regulator of excitatory synaptic physiology within the VMH. Moreover, they suggest that dysfunction in perisynaptic astrocyte processes may underlie reductions in excitatory synapse density and deficits in hyperglycemia-induced neuronal activity and excitatory transmission.

Discussion

In this study, we identified mGluR5 within VMH astrocytes as an essential regulator of excitatory synaptic transmission in PACAP^{+} neurons and peripheral glucose balance. In support,

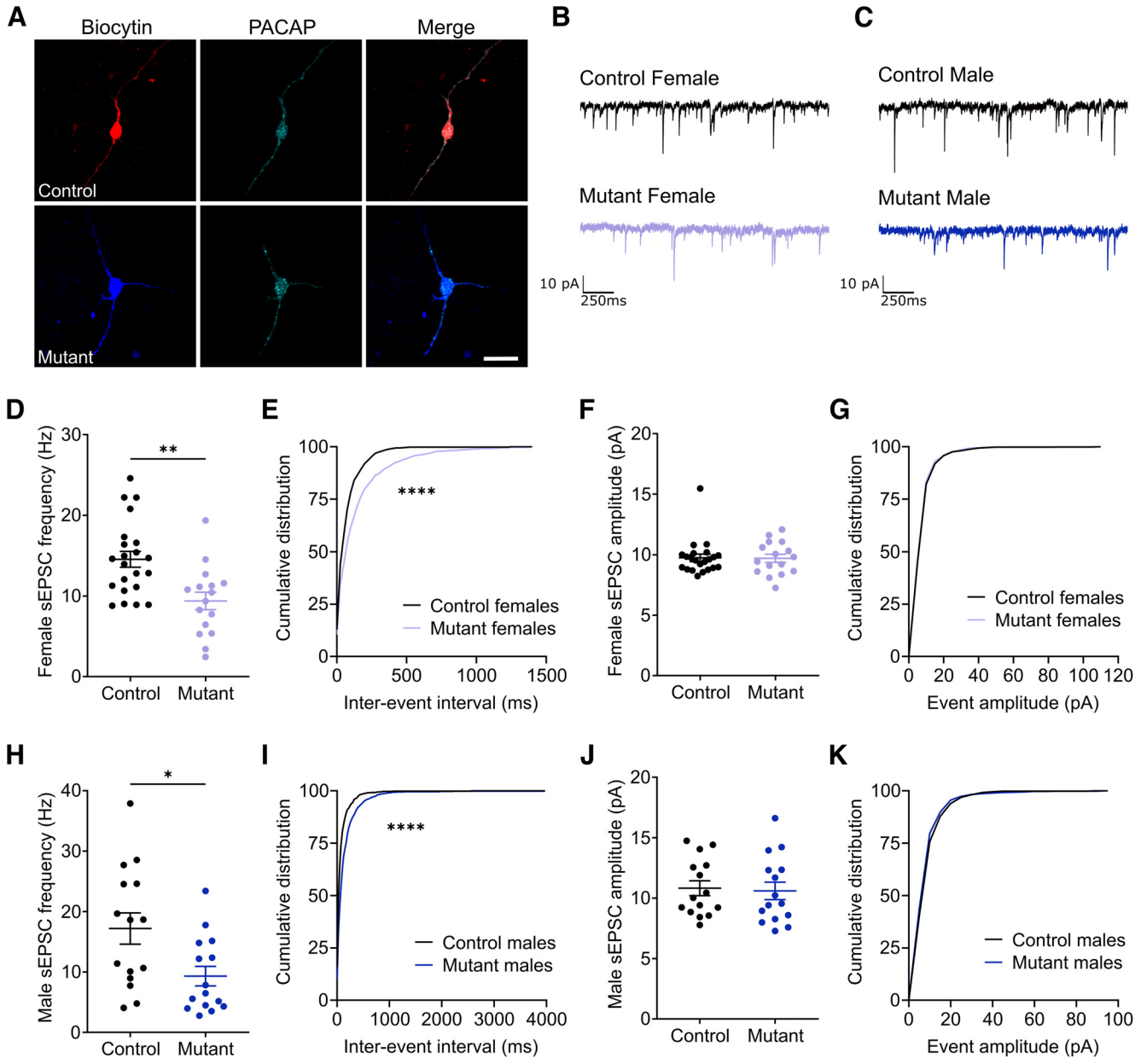

Figure 10. Excitatory drive onto VMH PACAP$^+$ neurons is reduced in the absence of astrocytic mGluR5. ***A***, Representative images of VMH cells filled with biocytin during whole-cell recordings and subsequently labeled with anti-PACAP (cyan). Scale bar, 50 μm. ***B***, Representative traces of sEPSCs in VMH PACAP$^+$ neurons from female mGluR5$^{GFAP\text{-}GFP}$ control and mGluR5$^{GFAP\text{-}Cre}$ mutant mice. ***C***, Representative traces of sEPSCs in VMH PACAP$^+$ neurons from male mGluR5$^{GFAP\text{-}GFP}$ control and mGluR5$^{GFAP\text{-}Cre}$ mutant mice. ***D***, Average sEPSC frequency of VMH PACAP$^+$ neurons from female controls ($n = 22$ cells from 6 animals) and mutants ($n = 16$ cells from 7 animals). Unpaired t test, $t_{(36)} = 3.490$, $^{**}p = 0.0013$. ***E***, Cumulative distribution of interevent interval generated from 50 random events per recorded cell for female controls ($n = 22$ cells from 6 animals) and mutants ($n = 16$ cells from 7 animals). Kolmogorov–Smirnov test, $^{****}p < 0.0001$. ***F***, Average sEPSC amplitude of VMH PACAP$^+$ neurons from female controls ($n = 22$ cells from 6 animals) and mutants ($n = 16$ cells from 7 animals). Unpaired t test, $t_{(36)} = 0.09{,}458$, $p = 0.93$. ***G***, Cumulative distribution of event amplitude generated from 50 random events per recorded cell for female controls ($n = 22$ cells from 6 animals) and mutants ($n = 16$ cells from 7 animals). Kolmogorov–Smirnov test, $p = 0.27$. ***H***, Average sEPSC frequency of VMH PACAP$^+$ neurons from male controls ($n = 15$ cells from 5 animals) and mutants ($n = 15$ cells from 5 animals). Unpaired t test, $t_{(28)} = 2.588$ $^*p = 0.015$. ***I***, Cumulative distribution of interevent interval generated from 50 random events per recorded cell for male controls ($n = 15$ cells from 5 animals) and mutants ($n = 15$ cells from 5 animals). Kolmogorov–Smirnov test, $^{****}p < 0.0001$. ***J***, Average sEPSC amplitude of VMH PACAP$^+$ neurons from male controls ($n = 15$ cells from 5 animals) and mutants ($n = 15$ cells from 5 animals). Unpaired t test, $t_{(28)} = 0.2315$, $p = 0.82$. ***K***, Cumulative distribution of event amplitude generated from 50 random events per recorded cell for male controls ($n = 15$ cells from 5 animals) and mutants ($n = 15$ cells from 5 animals). Kolmogorov–Smirnov test, $p = 0.13$.

selective depletion of astrocytic mGluR5 in the VMH of mice diminished the excitatory drive onto PACAP$^+$ neurons in this region, reduced activity responses of these cells to a glucose challenge, and enhanced insulin secretion and glucose tolerance. Based on the findings, we propose that astrocytic mGluR5 in the VMH increases the excitatory drive onto PACAP neurons during responses to acute hyperglycemia to limit insulin secretion and prevent excessive glucose disposal and hypoglycemia. Furthermore, the results indicate that mGluR5 in VMH astrocytes plays key roles regulating adipocyte size and sympathetic output to gonadal white adipose tissue. In total, our data inform mechanisms for astrocytic control of ventromedial hypothalamic activity regulating metabolic homeostasis.

Limited studies have examined the role of mGluR5 in the control of energy and glucose balance, and no studies addressed its role specific to astrocytes. Interestingly, adult mGluR5-null

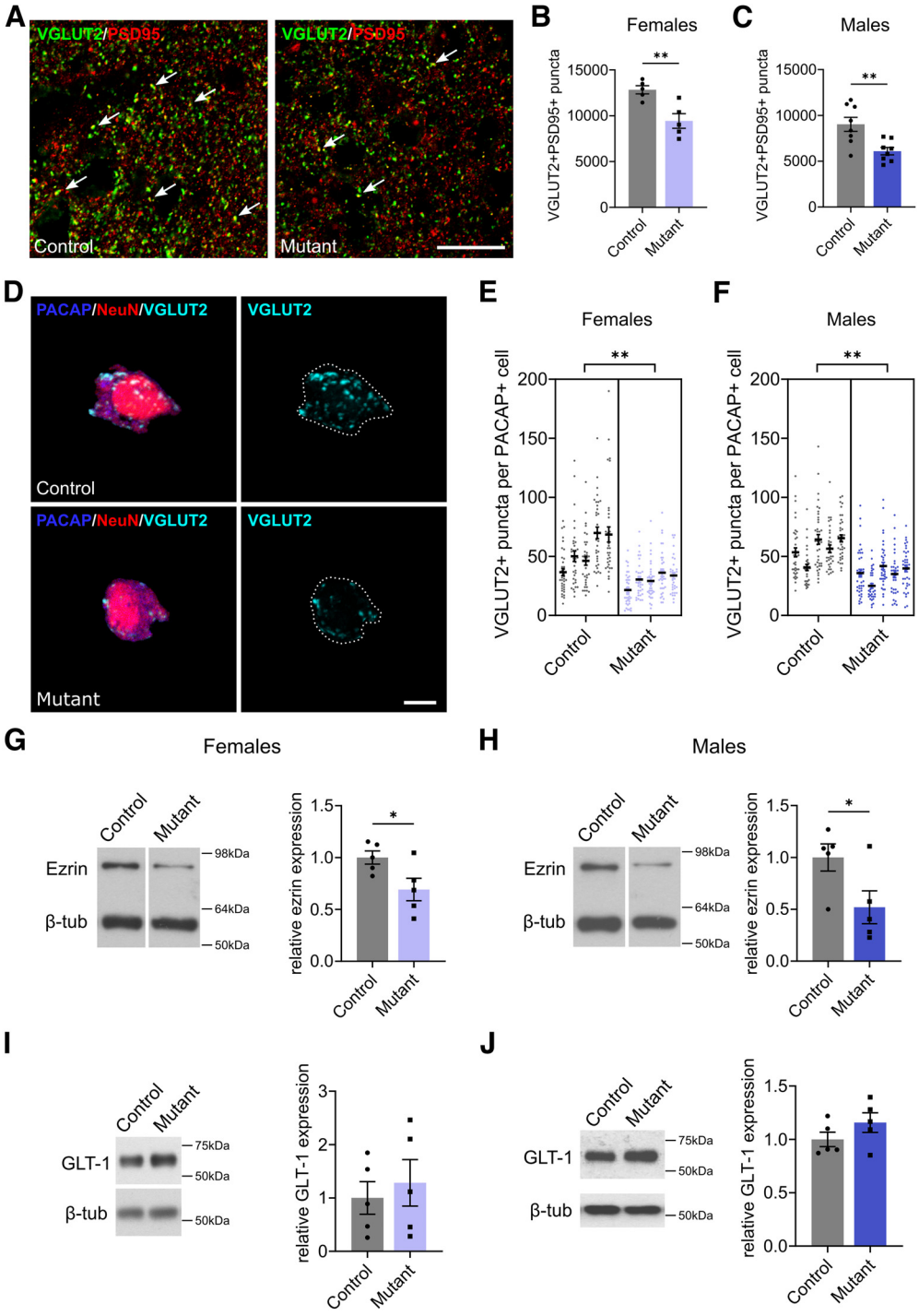

Figure 11. Depletion of mGluR5 from VMH astrocytes disrupts excitatory synaptic physiology. ***A***, Representative image of VGLUT2 (green) and PSD95 (red) coimmunolabeling in the VMH of female mGluR5$^{GFAP\text{-}GFP}$ control and mGluR5$^{GFAP\text{-}Cre}$ mutant mice. Arrows point to overlapping VGLUT2/PSD95 puncta, indicating an excitatory synapse. Scale bar, 25 μm. ***B***, Quantification of colocalized VGLUT2 and PSD95 puncta in the VMH of female control and mutant mice ($n = 5$ mice/group). Unpaired t test, $t_{(8)} = 3.719$, $^{**}p = 0.0059$. ***C***, Quantification of colocalized VGLUT2 and PSD95 puncta in the VMH of male control and mutant mice ($n = 8$ mice/group). Unpaired t test, $t_{(14)} = 3.383$, $^{**}p = 0.0045$. ***D***, Representative images from male mGluR5$^{GFAP\text{-}GFP}$ controls and mGluR5$^{GFAP\text{-}Cre}$ mutants of VGLUT2^{+} (cyan) immunolabeled puncta on the surface of VMH PACAP^{+} (dark blue) neurons, using NeuN (red) stain for 3D reconstruction of cell soma. Scale bar: 10 μm. ***E***, Quantification of VGLUT2^{+} puncta on PACAP^{+} neurons in the VMH of female controls and mutants ($n = 33$–38 cells/animal, 5 animals/group). Nested t test, $t_{(8)} = 3.457$, $^{**}p = 0.0086$. ***F***, Quantification of VGLUT2^{+} puncta on PACAP^{+} neurons in the VMH of male controls and mutants ($n = 32$–39 cells/animal, 5 animals/group). Nested t test, $t_{(8)} = 3.884$, $^{**}p = 0.0046$. ***G***, Representative Western blot measuring ezrin protein content and quantification of ezrin protein expression in the VMH of female controls and mutants ($n = 5$ animals/group). Control and mutant lanes taken from the same gel. Unpaired t test, $t_{(8)} = 2.448$, $^{*}p = 0.040$. ***H***, Representative Western blot measuring ezrin protein content and quantification of ezrin protein expression in the VMH of male controls and mutants ($n = 5$ animals/group). Control and mutant lanes taken from the same gel. Unpaired t test, $t_{(8)} = 2.335$, $^{*}p = 0.048$. ***I***, Representative Western blot measuring GLT-1 protein content and quantification of GLT-1 protein expression in the VMH of female controls and mutants ($n = 5$ animals/group). Unpaired t test, $t_{(8)} = 0.5348$, $p = 0.60$. ***J***, Representative Western blot measuring GLT-1 protein content and quantification of GLT-1 protein expression in the VMH of male controls and mutants ($n = 5$ animals/group). Unpaired t test, $t_{(8)} = 1.373$, $p = 0.21$.

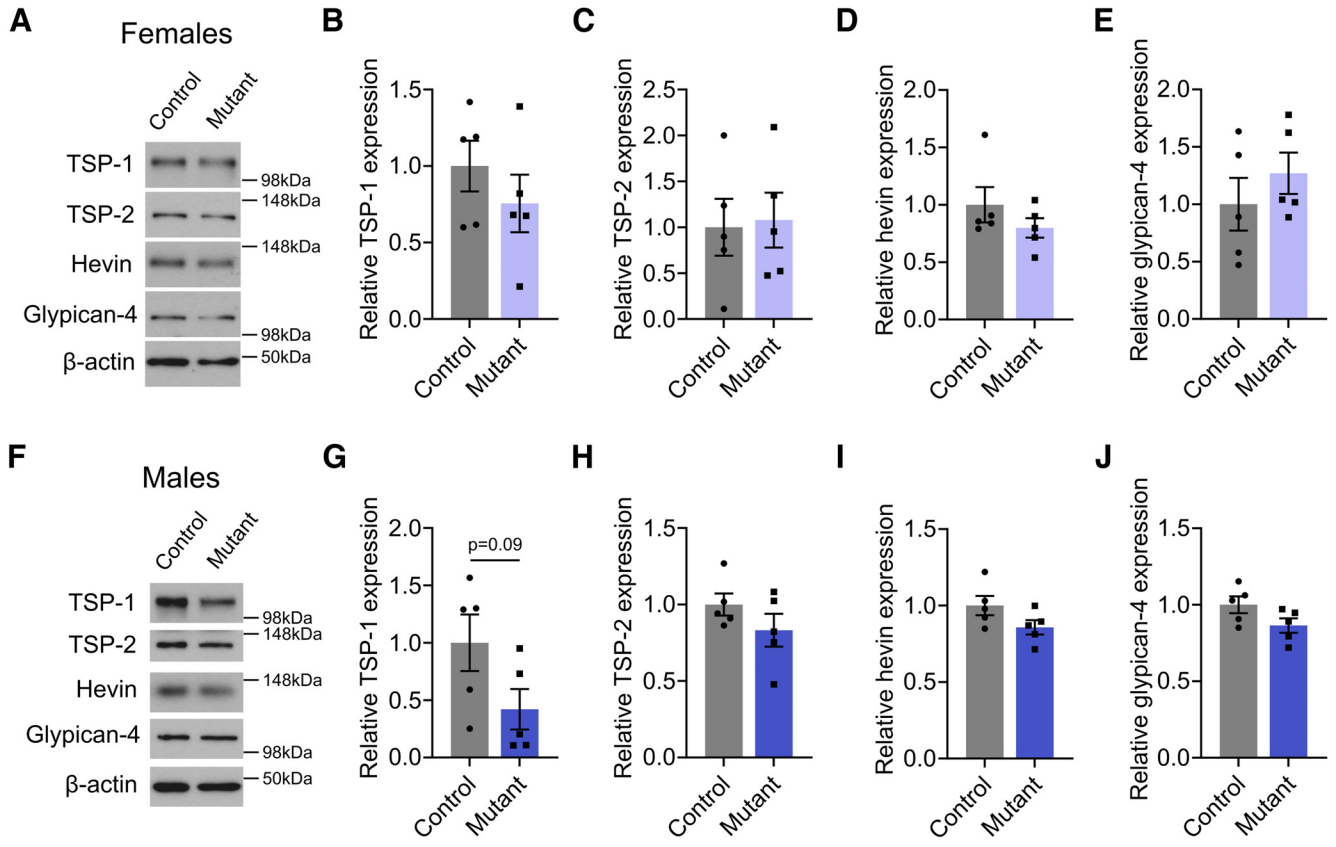

Figure 12. Depletion of astrocytic mGluR5 does not affect expression of synaptogenic markers in the VMH. ***A***, Representative Western blots measuring TSP-1, TSP-2, hevin, and glypican-4 expression with β-actin loading control from the VMH of female mGluR5$^{GFAP\text{-}GFP}$ control and mGluR5$^{GFAP\text{-}Cre}$ mutant mice. ***B***, Quantification of TSP-1 protein expression in female control and mutant mice ($n = 5$ animals/group). Unpaired t test, $t_{(8)} = 0.9724$, $p = 0.36$. ***C***, Quantification of TSP-2 protein expression in female control and mutant mice ($n = 5$ animals/group). Unpaired t test, $t_{(8)} = 0.1807$, $p = 0.86$. ***D***, Quantification of hevin protein expression in female control and mutant mice ($n = 5$ animals/group). Unpaired t test, $t_{(8)} = 1.152$, $p = 0.28$. ***E***, Quantification of glypican-4 protein expression in female control and mutant mice ($n = 5$ animals/group). Unpaired t test, $t_{(8)} = 0.9222$, $p = 0.38$. ***F***, Representative Western blots measuring TSP-1, TSP-2, hevin, and glypican-4 expression with β-actin loading control from the VMH of male mGluR5$^{GFAP\text{-}GFP}$ control and mGluR5$^{GFAP\text{-}Cre}$ mutant mice. ***G***, Quantification of TSP-1 protein expression in male control and mutant mice ($n = 5$ animals/group). Unpaired t test, $t_{(8)} = 1.912$, $p = 0.092$. ***H***, Quantification of TSP-2 protein expression in male control and mutant mice ($n = 5$ animals/group). Unpaired t test, $t_{(8)} = 1.298$, $p = 0.23$. ***I***, Quantification of hevin protein expression in male control and mutant mice ($n = 5$ animals/group). Unpaired t test, $t_{(8)} = 1.818$, $p = 0.11$. ***J***, Quantification of glypican-4 protein expression in male control and mutant mice ($n = 5$ animals/group). Unpaired t test, $t_{(8)} = 1.880$, $p = 0.097$.

mice are leaner than wild-type littermates despite exhibiting similar food intake, and mGluR1/5 agonism in the lateral hypothalamus stimulates feeding (Bradbury et al., 2005; Charles et al., 2014; Sánchez-Fuentes et al., 2016). However, the specific cell populations underlying the metabolic effects of mGluR5 remain elusive. We discovered that astrocytic mGluR5 in the VMH plays key roles regulating glucose homeostasis via body-weight-independent mechanisms in both female and male mice. Accordingly, mGluR5 depletion from VMH astrocytes resulted in enhanced glucose-stimulated insulin secretion and glucose tolerance without affecting body weight control, and this was associated with neuronal hypoactivity in this region. In contrast, we reported previously that selective depletion of mGluR5 in SF1^{+} neurons elicited glucose intolerance only in female mice, and this effect was also associated with reduced neuronal activity (Fagan et al., 2020). The opposite effects of perturbing mGluR5 on glycemic control illustrate its complex and context-dependent functions. Historically, studies examining VMH control of metabolic function have centered on SF1^{+} neurons because of their exclusivity to the VMH within the brain and the availability of reliable genetic tools to selectively manipulate this cell population (Bingham et al., 2006; Dhillon et al., 2006; Choi et al., 2013). However, it is important to note the diverse cellular composition of the VMH, which confers functional heterogeneity and differentially affects glucose production and utilization in the periphery (Shimazu and Minokoshi, 2017; Tu et al., 2022). Therefore, a major finding of this work is the identification of a specific neuronal population expressing PACAP in the VMH that appears to mediate the effects of astrocytic mGluR5 on glucose homeostasis.

In addition to alterations in glucose balance control, depletion of astrocytic mGluR5 in the VMH elicited reductions in adipocyte size in gonadal white adipose tissue in both female and male mice. This was accompanied by significant elevations in norepinephrine content specifically in gWAT, indicating increased sympathetic tone in this fat depot. This is notable as the VMH has long been established to affect lipid metabolism through sympathetic outflow to adipose tissues (Takahashi and Shimazu, 1981, 1982). Specifically, NE released onto WAT by sympathetic fibers activates adrenergic pathways controlling lipid mobilization, adipokine production and secretion, and adipocyte growth and proliferation (Bartness et al., 2014; Stenkula and Erlanson-Albertsson, 2018; Ryu and Buettner, 2019). The selective effect of astrocytic mGluR5 on sympathetic tone in gWAT is likely related to the finding that gWAT and iWAT fat pads receive distinct, largely nonoverlapping patterns of sympathetic nervous system innervation that can be differentially regulated (Youngstrom and Bartness, 1995; Nguyen et al., 2014). Adipose tissue is highly dynamic in the number and size of its adipocytes,

and its sympathetic innervation can drive these changes via induction of lipolysis or inhibition of WAT growth (Shi et al., 2005; Bartness et al., 2014). Although VMH stimulation has been shown to promote lipolysis through sympathetic innervation (Takahashi and Shimazu, 1981), NE signaling in WAT may trigger both prolipolytic and anti-lipolytic pathways depending on the balance of stimulatory β-adrenergic and inhibitory α2-adrenergic receptors activated (Bartness et al., 2014). We did not detect alterations in triglyceride content in gWAT or circulating levels of glycerol or free fatty acids in mutant mice, suggesting lipid mobilization in this depot is unaffected. In rats, normal adipose tissue growth during aging is accomplished through increases in both cell number and cell size, with gonadal WAT growing primarily because of the latter (DiGirolamo et al., 1998). Sympathetic denervation, which reduces tissue NE content, increases gWAT mass via increased adipocyte size without affecting total cell number (Shi et al., 2005), suggesting that NE signaling inhibits gWAT growth through control of cell size. In our model, increased sympathetic tone in gWAT of mGluR5$^{GFAP\text{-}Cre}$ mutant animals likely reduces adipocyte size through increased inhibition of WAT growth without affecting lipolysis.

Because astrocytes can both detect and modulate excitatory activity via mGluR5 present in perisynaptic processes (D'Ascenzo et al., 2007; Parri et al., 2010; Panatier et al., 2011), we probed whether depleting astrocytic mGluR5 affected VMH excitatory transmission. This was indeed the case as indicated by a reduction in frequency of sEPSCs in neurons in the dorsomedial and central VMH. Considering that improved glucose tolerance in mGluR5$^{GFAP\text{-}Cre}$ mice was accompanied by augmented glucose-stimulated insulin secretion, we focused our attention on VMH PACAP^{+} neurons, which inhibit insulin secretion without affecting glucagon levels (Khodai et al., 2018). In mGluR5$^{GFAP\text{-}Cre}$ mice, the number of c-fos–expressing PACAP^{+} cells is reduced in the VMH, indicating blunted neuronal activity at 60 min after glucose administration. Interestingly, blood levels of glucose are falling at this time point compared with peak levels following glucose delivery. Decreased sEPSC frequency observed in VMH PACAP^{+} neurons in mGluR5$^{GFAP\text{-}Cre}$ mutants suggests a presynaptic locus of astrocytic mGluR5-mediated regulation. In agreement, there was a reduced number of excitatory presynaptic contacts onto PACAP^{+} cell soma within the VMH of astrocytic mGluR5 mutants. Collectively, the findings suggest that astrocytic mGluR5 mediates increases in the activity of VMH PACAP^{+} neurons following glucose influx. Considering the known effects of these cells limiting insulin secretion, it is possible that this represents a mechanism preventing excessive glucose disposal and hypoglycemia. It remains unclear whether the diminished excitability of PACAP neurons in mGluR5$^{GFAP\text{-}Cre}$ mutants also contributes to the alterations in gWAT exhibited by these mice. Considering the ability of astrocytes to regulate hundreds of thousands of synapses, it is possible that alterations in the activity of other neuronal cell populations in the VMH underlie these metabolic changes.

Astrocytes promote synapse formation and remodeling through the release of synaptogenic molecules. Moreover, transient induction of mGluR5 in cortical astrocytes induced expression of TSP-1, glypican-4, and hevin, astrocyte-secreted factors that regulate excitatory synapse formation (Baldwin and Eroglu, 2017; Danjo et al., 2022). However, we found that depletion of astrocytic mGluR5 did not significantly affect VMH levels of any of these factors. Astrocytes possess highly plastic perisynaptic processes that physically interact with neurons to regulate synapse formation and stability. Notably, metabolic cues such as postprandial hyperglycemia can alter astrocytic synapse coverage to adapt synaptic activity in response to these nutrient content changes (Bernardinelli et al., 2014; Chung et al., 2015; Nuzzaci et al., 2020). Group 1 mGluR-dependent activity, which includes mGluR5, facilitates PAP plasticity and motility associated with synapse stabilization, and this requires the cytoskeletal linker protein ezrin (Lavialle et al., 2011; Bernardinelli et al., 2014; Perez-Alvarez et al., 2014). Expression of ezrin in the adult mammalian brain is restricted to astrocytes, where it localizes preferentially to PAPs (Haseleu et al., 2013; Derouiche and Geiger, 2019). Interestingly, ezrin colocalizes with mGluR5 in PAPs in the suprachiasmatic nucleus of the hypothalamus (Lavialle et al., 2011). Here, we showed that mGluR5$^{GFAP\text{-}Cre}$ mutants exhibited significantly decreased ezrin expression in the VMH. Therefore, it is possible that the ability of PAPs to remodel to stabilize excitatory synapses might be compromised in astrocytes depleted of mGluR5, resulting in decreased density of excitatory synapses. In the ischemic mouse brain, ezrin-mediated formation of PAPs has a protective effect on synapse stability, increasing excitatory synapse numbers following severe reduction by injury (Diaz et al., 2019). In the context of acute hyperglycemia, it is likely that the excitatory synapse deficits displayed in mGluR5$^{GFAP\text{-}Cre}$ mutants render PACAP^{+} neurons in the VMH unable to respond to changes in peripheral glucose levels as needed.

In summary, we report a multifaceted and critical role of astrocytic mGluR5 in the VMH for regulating peripheral metabolic homeostasis in both female and male mice. Furthermore, we show that astrocytic mGluR5 is a critical player in the regulation of excitatory transmission and synaptic function underlying glucose balance. We propose that during acute hyperglycemia, astrocytic mGluR5 acts as a sensor of glucose-induced glutamatergic activity in the VMH and subsequently mediates homeostatic increases in excitatory tone onto PACAP^{+} cells, which for their part, restrain insulin secretion to prevent excessive glucose removal from the circulation. These studies inform mechanisms that may be perturbed in metabolic disorders such as diabetes and provide further evidence for the importance of and need for studying astrocytic regulation of hypothalamic circuits involved in systemic metabolism.

References

Ameroso D, Meng A, Chen S, Felsted J, Dulla CG, Rios M (2022) Astrocytic BDNF signaling within the ventromedial hypothalamus regulates energy homeostasis. Nat Metab 4:627–643.

Araque A, Carmignoto G, Haydon PG, Oliet SHR, Robitaille R, Volterra A (2014) Gliotransmitters travel in time and space. Neuron 81:728–739.

Baldwin KT, Eroglu C (2017) Molecular mechanisms of astrocyte-induced synaptogenesis. Curr Opin Neurobiol 45:113–120.

Bartness TJ, Liu Y, Shrestha YB, Ryu V (2014) Neural innervation of white adipose tissue and the control of lipolysis. Front Neuroendocrinol 35:473–493.

Bernardinelli Y, Randall J, Janett E, Nikonenko I, König S, Jones EV, Flores CE, Murai KK, Bochet CG, Holtmaat A, Muller D (2014) Activity-dependent structural plasticity of perisynaptic astrocytic domains promotes excitatory synapse stability. Curr Biol 24:1679–1688.

Bingham NC, Verma-Kurvari S, Parada LF, Parker KL (2006) Development of a steroidogenic factor 1/Cre transgenic mouse line. Genesis 44:419–424.

Bradbury MJ, Campbell U, Giracello D, Chapman D, King C, Tehrani L, Cosford NDP, Anderson J, Varney MA, Strack AM (2005) Metabotropic glutamate receptor mGlu5 is a mediator of appetite and energy balance in rats and mice. J Pharmacol Exp Ther 313:395–402.

Bushong EA, Martone ME, Jones YZ, Ellisman MH (2002) Protoplasmic astrocytes in CA1 stratum radiatum occupy separate anatomical domains. J Neurosci 22:183–192.

Cai Z, Schools GP, Kimelberg HK (2000) Metabotropic glutamate receptors in acutely isolated hippocampal astrocytes: developmental changes of mGluR5 mRNA and functional expression. Glia 29:70–80.

Charles JR, Duva MA, Ramirez GJ, Lara RL, Yang CR, Stanley BG (2014) Activation of lateral hypothalamic mGlu1 and mGlu5 receptors elicits feeding in rats. Neuropharmacology 79:59–65.

Choi Y-H, Fujikawa T, Lee J, Reuter A, Kim KW (2013) Revisiting the ventral medial nucleus of the hypothalamus: the roles of SF-1 neurons in energy homeostasis. Front Neurosci 7:71.

Chung WS, Allen NJ, Eroglu C (2015) Astrocytes control synapse formation, function, and elimination. Cold Spring Harb Perspect Biol 7:a020370.

Danbolt NC, Storm-Mathisen J, Kanner BI (1992) An [Na+ + K+]coupled l-glutamate transporter purified from rat brain is located in glial cell processes. Neuroscience 51:295–310.

Danjo Y, Shigetomi E, Hirayama YJ, Kobayashi K, Ishikawa T, Fukazawa Y, Shibata K, Takanashi K, Parajuli B, Shinozaki Y, Kim SK, Nabekura J, Koizumi S (2022) Transient astrocytic mGluR5 expression drives synaptic plasticity and subsequent chronic pain in mice. J Exp Med 219:e20210989.

D'Ascenzo M, Fellin T, Terunuma M, Revilla-Sanchez R, Meaney DF, Auberson YP, Moss SJ, Haydon PG (2007) mGluR5 stimulates gliotransmission in the nucleus accumbens. Proc Natl Acad Sci U S A 104:1995–2000.

Derouiche A, Geiger KD (2019) Perspectives for ezrin and radixin in astrocytes: kinases, functions and pathology. Int J Mol Sci 20:3776.

Devaraju P, Sun MY, Myers TL, Lauderdale K, Fiacco TA (2013) Astrocytic group I mGluR-dependent potentiation of astrocytic glutamate and potassium uptake. J Neurophysiol 109:2404–2414.

Dhillon H, Zigman JM, Ye C, Lee CE, McGovern RA, Tang V, Kenny CD, Christiansen LM, White RD, Edelstein EA, Coppari R, Balthasar N, Cowley MA, Chua S, Elmquist JK, Lowell BB (2006) Leptin directly activates SF1 neurons in the VMH, and this action by leptin is required for normal body-weight homeostasis. Neuron 49:191–203.

Diaz A, Merino P, Manrique LG, Cheng L, Yepes M (2019) Urokinase-type plasminogen activator (uPA) protects the tripartite synapse in the ischemic brain via ezrin-mediated formation of peripheral astrocytic processes. J Cereb Blood Flow Metab 39:2157–2171.

DiGirolamo M, Fine JB, Tagra K, Rossmanith R (1998) Qualitative regional differences in adipose tissue growth and cellularity in male Wistar rats fed *ad libitum*. Am J Physiol Regul Integr Comp Physiol 274:R1460–R1467.

Dunn-Meynell AA, Govek E, Levin BE (1997) Intracarotid glucose selectively increases Fos-like immunoreactivity in paraventricular, ventromedial and dorsomedial nuclei neurons. Brain Res 748:100–106.

Fagan MP, Ameroso D, Meng A, Rock A, Maguire J, Rios M (2020) Essential and sex-specific effects of mGluR5 in ventromedial hypothalamus regulating estrogen signaling and glucose balance. Proc Natl Acad Sci 117:19566–19577.

García-Cáceres C, et al. (2016) Astrocytic insulin signaling couples brain glucose uptake with nutrient availability. Cell 166:867–880.

Garfield AS, Shah BP, Madara JC, Burke LK, Patterson CM, Flak J, Neve RL, Evans ML, Lowell BB, Myers MG, Heisler LK (2014) A parabrachial-hypothalamic cholecystokinin neurocircuit controls counterregulatory responses to hypoglycemia. Cell Metab 20:1030–1037.

Halassa MM, Fellin T, Takano H, Dong JH, Haydon PG (2007) Synaptic islands defined by the territory of a single astrocyte. J Neurosci 27:6473–6477.

Haque MS, Minokoshi Y, Hamai M, Iwai M, Horiuchi M, Shimazu T (1999) Role of the sympathetic nervous system and insulin in enhancing glucose uptake in peripheral tissues after intrahypothalamic injection of leptin in rats. Diabetes 48:1706–1712.

Haseleu J, Anlauf E, Blaess S, Endl E, Derouiche A (2013) Studying subcellular detail in fixed astrocytes: dissociation of morphologically intact glial cells (DIMIGs). Front Cell Neurosci 7:54.

Hawke Z, Ivanov TR, Bechtold DA, Dhillon H, Lowell BB, Luckman SM (2009) PACAP neurons in the hypothalamic ventromedial nucleus are targets of central leptin signaling. J Neurosci 29:14828–14835.

Kang L, Routh VH, Kuzhikandathil EV, Gaspers LD, Levin BE (2004) Physiological and molecular characteristics of rat hypothalamic ventromedial nucleus glucosensing neurons. Diabetes 53:549–559.

Khodai T, Nunn N, Worth AA, Feetham CH, Belle MDC, Piggins HD, Luckman SM (2018) PACAP Neurons in the ventromedial hypothalamic nucleus are glucose inhibited and their selective activation induces hyperglycaemia. Front Endocrinol (Lausanne) 9:632.

Kim JG, et al. (2014) Leptin signaling in astrocytes regulates hypothalamic neuronal circuits and feeding. Nat Neurosci 17:908–910.

King BM (2006) The rise, fall, and resurrection of the ventromedial hypothalamus in the regulation of feeding behavior and body weight. Physiol Behav 87:221–244.

Kumon A, Takahashi A, Hara T, Shimazu T (1976) Mechanism of lipolysis induced by electrical stimulation of the hypothalamus in the rabbit. J Lipid Res 17:551–558.

Lavialle M, Aumann G, Anlauf E, Pröls F, Arpin M, Derouiche A (2011) Structural plasticity of perisynaptic astrocyte processes involves ezrin and metabotropic glutamate receptors. Proc Natl Acad Sci U S A 108:12915–12919.

Lindberg D, Chen P, Li C (2013) Conditional viral tracing reveals that steroidogenic factor 1-positive neurons of the dorsomedial subdivision of the ventromedial hypothalamus project to autonomic centers of the hypothalamus and hindbrain. J Comp Neurol 521:3167–3190.

Liu J, Bisschop PH, Eggels L, Foppen E, Ackermans MT, Zhou JN, Fliers E, Kalsbeek A (2013) Intrahypothalamic estradiol regulates glucose metabolism via the sympathetic nervous system in female rats. Diabetes 62:435–443.

Meek TH, Nelson JT, Matsen ME, Dorfman MD, Guyenet SJ, Damian V, Allison MB, Scarlett JM, Nguyen HT, Thaler JP, Olson DP, Myers MG, Schwartz MW, Morton GJ (2016) Functional identification of a neurocircuit regulating blood glucose. Proc Natl Acad Sci U S A 113:E2073–E2082.

Minokoshi Y, Okano Y, Shimazu T (1994) Regulatory mechanism of the ventromedial hypothalamus in enhancing glucose uptake in skeletal muscles. Brain Res 649:343–347.

Morel L, Higashimori H, Tolman M, Yang Y (2014) VGluT1+ neuronal glutamatergic signaling regulates postnatal developmental maturation of cortical protoplasmic astroglia. J Neurosci 34:10950–10962.

Nguyen NLT, Randall J, Banfield BW, Bartness TJ (2014) Central sympathetic innervations to visceral and subcutaneous white adipose tissue. Am J Physiol Regul Integr Comp Physiol 306:R375–R386.

Nuzzaci D, et al. (2020) Postprandial hyperglycemia stimulates neuroglial plasticity in hypothalamic POMC neurons after a balanced meal. Cell Rep 30:3067–3078.e5.

Oliet SH, Piet R, Poulain DA (2001) Control of glutamate clearance and synaptic efficacy by glial coverage of neurons. Science 292:923–926.

Panatier A, Vallée J, Haber M, Murai KK, Lacaille J-C, Robitaille R (2011) Astrocytes are endogenous regulators of basal transmission at central synapses. Cell 146:785–798.

Parri HR, Gould TM, Crunelli V (2010) Sensory and cortical activation of distinct glial cell subtypes in the somatosensory thalamus of young rats. Eur J Neurosci 32:29–40.

Perez-Alvarez A, Navarrete M, Covelo A, Martin ED, Araque A (2014) Structural and functional plasticity of astrocyte processes and dendritic spine interactions. J Neurosci 34:12738–12744.

Ramseyer VD, Granneman JG (2016) Adrenergic regulation of cellular plasticity in brown, beige/brite and white adipose tissues. Adipocyte 5:119–129.

Routh VH, Hao L, Santiago AM, Sheng Z, Zhou C (2014) Hypothalamic glucose sensing: making ends meet. Front Syst Neurosci 8:236.

Ryu V, Buettner C (2019) Fat cells gobbling up norepinephrine? PLoS Biol 17:e3000138.

Saito M, Minokoshi Y, Shimazu T (1989) Accelerated norepinephrine turnover in peripheral tissues after ventromedial hypothalamic stimulation in rats. Brain Res 481:298–303.

Sánchez-Fuentes A, Marichal-Cancino BA, Méndez-Díaz M, Becerril-Meléndez AL, Ruiz-Contreras AE, Prospéro-Garcia O (2016) mGluR1/5 activation in the lateral hypothalamus increases food intake via the endocannabinoid system. Neurosci Lett 631:104–108.

Shi H, Song CK, Giordano A, Cinti S, Bartness TJ (2005) Sensory or sympathetic white adipose tissue denervation differentially affects depot growth and cellularity. Am J Physiol Regul Integr Comp Physiol 288:R1028–R10237.

Shimazu T, Minokoshi Y (2017) Systemic glucoregulation by glucose-sensing neurons in the ventromedial hypothalamic nucleus (VMH). J Endocr Soc 1:449–459.

Shimazu T, Sudo M, Minokoshi Y, Takahashi A (1991) Role of the hypothalamus in insulin-independent glucose uptake in peripheral tissues. Brain Res Bull 27:501–504.

Stanley SA, Kelly L, Latcha KN, Schmidt SF, Yu X, Nectow AR, Sauer J, Dyke JP, Dordick JS, Friedman JM (2016) Bidirectional electromagnetic control of the hypothalamus regulates feeding and metabolism. Nature 531:647–650.

Stenkula KG, Erlanson-Albertsson C (2018) Adipose cell size: importance in health and disease. Am J Physiol Regul Integr Comp Physiol 315:R284–R295.

Sun MY, Devaraju P, Xie AX, Holman I, Samones E, Murphy TR, Fiacco TA (2014) Astrocyte calcium microdomains are inhibited by Bafilomycin A1 and cannot be replicated by low-level Schaffer collateral stimulation in situ. Cell Calcium 55:1–16.

Sun W, McConnell E, Pare J-F, Xu Q, Chen M, Peng W, Lovatt D, Han X, Smith Y, Nedergaard M (2013) Glutamate-dependent neuroglial calcium signaling differs between young and adult brain. Science 339:197–200.

Sun W, Cornwell A, Li J, Peng S, Joana Osorio M, Aalling N, Wang S, Benraiss A, Lou N, Goldman SA, Nedergaard M (2017) SOX9 is an astrocyte-specific nuclear marker in the adult brain outside the neurogenic regions. J Neurosci 37:4493–4507.

Takahashi A, Shimazu T (1981) Hypothalamic regulation of lipid metabolism in the rat: effect of hypothalamic stimulation on lipolysis. J Auton Nerv Syst 4:195–205.

Takahashi A, Shimazu T (1982) Hypothalamic regulation of lipid metabolism in the rat: effect of hypothalamic stimulation on lipogenesis. J Auton Nerv Syst 6:225–235.

Toda C, Kim JD, Impellizzeri D, Cuzzocrea S, Liu Z-W, Diano S (2016) UCP2 regulates mitochondrial fission and ventromedial nucleus control of glucose responsiveness. Cell 164:872–883.

Tu L, Fukuda M, Tong Q, Xu Y (2022) The ventromedial hypothalamic nucleus: watchdog of whole-body glucose homeostasis. Cell Biosci 12:71.

Ullian EM, Sapperstein SK, Christopherson KS, Barres BA (2001) Control of synapse number by glia. Science 291:657–661.

Van Den Pol AN, Romano C, Ghosh P (1995) Metabotropic glutamate receptor mGluR5 subcellular distribution and developmental expression in hypothalamus. J Comp Neurol 362:134–150.

Vermeiren C, Najimi M, Vanhoutte N, Tilleux S, De Hemptinne I, Maloteaux J-M, Hermans E (2005) Acute up-regulation of glutamate uptake mediated by mGluR5a in reactive astrocytes. J Neurochem 94:405–416.

Wu Q, Lemus MB, Stark R, Bayliss JA, Reichenbach A, Lockie SH, Andrews ZB (2014) The temporal pattern of cfos activation in hypothalamic, cortical, and brainstem nuclei in response to fasting and refeeding in male mice. Endocrinology 155:840–853.

Youngstrom TG, Bartness TJ (1995) Catecholaminergic innervation of white adipose tissue in Siberian hamsters. Am J Physiol Regul Integr Comp Physiol 268:R744–R751.